Structure and mechanism of an active lipid-linked oligosaccharide flippase

Author(s):
Perez, Camilo; Gerber, Sabina; Boilevin, Jérémy; Bucher, Monika; Darbre, Tamis; Aebi, Markus; Reymond, Jean-Louis; Locher, Kaspar P.

Publication date:
2015

Permanent link:
https://doi.org/10.3929/ethz-b-000104075

Originally published in:
Nature 524(7566), https://doi.org/10.1038/nature14953

Funding acknowledgement:
146191 - Reaction mechanism of bacterial ABC transporters and oligosaccharyltransferase (SNF)

Structure and mechanism of an ATP-driven lipid-linked-oligosaccharide flippase

Camilo Perez[1], Sabina Gerber[1,†], Jérémy Boilevin[2], Monika Bucher[1], Tamis Darbre[2], Markus Aebi[3], Jean-Louis Reymond[2], Kaspar P. Locher[1]

[1]Department of Biology, Institute of Molecular Biology and Biophysics, ETH Zürich, CH-8093 Zürich, Switzerland.

[2]Department of Chemistry and Biochemistry, University of Berne, CH-3012 Berne, Switzerland.

[3]Department of Biology, Institute of Microbiology, ETH Zürich, CH-8093 Zürich, Switzerland.

[†]Present address: GlycoVaxyn AG, Grabenstrasse 3, 8952 Schlieren, Switzerland.

Abbreviated title: Glycolipid flipping by PglK

Correspondence and requests for materials should be addressed to K.P.L. (email: locher@mol.biol.ethz.ch).

The flipping of membrane-embedded lipids containing large, polar head-groups is slow and energetically unfavorable and therefore catalyzed by flippases, whose mechanisms are currently unknown. A prominent example is the flipping of lipid-linked oligosaccharides (LLO) that serve as donors in N-linked protein glycosylation. In *Campylobacter jejuni*, LLO flipping is catalyzed by the ABC transporter PglK. Here we present a mechanism of PglK-catalyzed LLO flipping based on crystal structures in distinct states, a newly devised *in vitro* flipping assay, and *in vivo* studies. PglK can adopt inward- and outward-facing conformations *in vitro*, but only outward-facing states are required for flipping. While the oligosaccharide-pyrophosphate head-group enters the translocation cavity and interacts with a belt of positively charged side chains, the lipidic polyprenyl tail binds and activates the transporter but remains exposed to the lipid bilayer during the reaction. The proposed mechanism is distinct from the paradigmatic alternating-access model applied to other transporters.

The translocation of lipids across the membrane bilayer, termed flipping, is essential to maintain lipid asymmetry and required for processes such as signaling, vesicle formation in the secretory and endocytic pathways, the regulation of membrane protein activity, and asparagine-linked protein glycosylation[1-6]. In animals, loss of trans-bilayer lipid asymmetry has been related to processes including blood coagulation[7], macrophage recognition[8] and apoptosis[9]. In bacteria, precursors of cell wall components are coupled to lipid carriers and exported by flippases, processes that are essential for cell wall assembly[10-12]. Flipping reactions are catalyzed by active or passive transporters[13]. These include energy-independent scramblases that randomize the distribution of lipids across the bilayer[14,15], proton- or sodium-driven secondary antiporters[16], and ATP-driven, vectorial transporters that actively translocate specific lipids from one leaflet to the other. The latter include P4-ATPases[17] and ATP-binding cassette (ABC) transporters[13,18].

In eukaryotes, the lipid-linked-oligosaccharide (LLO) $Man_5GlcNAc_2$-PP-dolichol is flipped from the cytosolic side to the lumen of the endoplasmic reticulum (ER) membrane, where the oligosaccharide is transferred to asparagine residues of nascent polypeptide chains in protein N-glycosylation[1,2]. A chemically similar LLO ($GlcGalNAc_5$Bac-PP-Undecaprenyl, **Extended Data Fig. 1**) is flipped during protein N-glycosylation in the human pathogen *Campylobacter jejuni*[19,20]. The responsible flippase, PglK, is a homo-dimeric ABC transporter and an essential component of the bacterial protein N-glycosylation machinery[21]. The translocated LLO is handed over to the oligosaccharyltransferase PglB, which catalyzes the oligosaccharide transfer

to acceptor proteins[22]. Undecaprenyl-pyrophosophate is subsequently hydrolyzed to the mono-phosphate by undecaprenyl-pyrophosphatase[23] (**Extended Data Fig. 2**).

Despite extensive research, remarkably little is known about the mechanism of active, flippase-catalyzed lipid translocation. This is in part due to the absence of structural information. To date, structural data is only available for the bacterial lipid-A-core flippase MsbA[18,24], but no reliable mechanism of lipid A-core flipping could be deduced. In addition to the scarcity of structures, there are few reliable *in vitro* assays that allow the study of native substrate flipping.

To understand the mechanism of ATP-driven LLO flipping, we have developed an *in vitro* flipping assay and determined crystal structures of *Campylobacter jejuni* PglK in inward- and outward-facing states. Our results suggest an un-anticipated flipping mechanism in which only the outward-facing conformations are relevant for the flipping process, allowing the passage of the oligosaccharide head-group through the transporter while the polyprenyl tail remains partially embedded in the lipid bilayer but attached to the surface of PglK. This newly proposed mechanism is adapted to the chemical nature of glycolipids that share large hydrophobic and hydrophilic portions and is distinct from the alternating-access model that underlies the mechanism of most primary and secondary transporters studied to date.

In vitro LLO flipping assay and PglK activity

Flipping of isoprenoid glycolipids has previously been investigated using radiolabeled natural lipids[25,26]. We determined PglK-catalyzed LLO flipping rates by exploiting the fact that PglK can process LLOs with shortened oligosaccharides both *in vivo* and *in vitro*[21,27,28]. For our assay, we co-reconstituted PglK with a tri-saccharide LLO (tLLO) containing the reducing-end bacillosamine and two GalNAc moieties into proteoliposomes (**Fig. 1A**). To determine ATP-driven, PglK-dependent tLLO flipping, the amount of tLLO molecules in the outer, accessible leaflet of the proteoliposomes was quantitated by radio-labeling using purified glycosyltransferase PglH[29-31], an enzyme of the *Campylobacter jejuni* N-glycosylation machinery that was shown to attach up to three GalNAc residues to the non-reducing end of LLO (**Extended Data Fig. 2**). We used excess UDP-GalNAc, thereby forcing three GalNAc molecules to be added to each tLLO molecules, allowing accurate determination of the flipping of tLLO to the interior of the liposomes (**Fig. 1B, Extended Data Fig. 9A**). The conversion of tLLO to the hexa-saccharide LLO was confirmed by transferring the oligosaccharides to fluorescently labeled acceptor peptides using purified oligosaccharyltransferase PglB, followed by SDS PAGE analysis[28,32,33]. PglK-catalyzed *in vitro* tLLO flipping was strictly dependent on ATP hydrolysis. A PglK mutant containing a glutamine residue in the Walker-B motif (E510Q)

exhibited a 92 ± 27 -fold decreased of flipping activity, in agreement with a strongly reduced *in vivo* activity (**Fig. 1C,D, Extended Data Fig. 3A**). The ATPase activity of PglK in the presence of LLO follows Michaelis-Menten kinetics, with a Km = 0.46 ± 0.08, matching the Km of ATP-dependent tLLO flipping of 0.36 ± 0.03 mM (**Fig. 1E**). This corroborates the interpretation that ATP hydrolysis is required and directly responsible for PglK-catalyzed LLO flipping. As was observed with other ABC transporters, the native substrate can stimulate the ATPase activity, although the structural basis of this phenomenon is not understood. PglK-catalyzed ATPase activity is stimulated ~2.5-fold both by full-length LLO and tLLO and both in detergent and liposomes, demonstrating that the terminal GalNAc at the non-reducing end of native LLO is not relevant for ATPase stimulation or flipping (**Fig. 1E-G**). Importantly, although the hydrolysis and flipping rates are almost 100-fold lower than wild type PglK, the ATPase activity of the E510Q mutant is also stimulated by LLO, in agreement with the observed (slow) flipping activities. Unlike related ABC transporters whose ATPase activity is stimulated in the presence of diverse drugs[34,35], PglK exhibits high specificity, as commonly used drugs such as verapamil, Hoechst33342, rhodamine 6G, and acrilflavin did not affect the ATPase rates of PglK (**Fig. 1G**). Addition of lipid A, known to stimulate MsbA[36], was also unable to stimulate the ATPase activity of PglK.

Structures of PglK in distinct states

To understand the structural basis of LLO flipping, we determined three crystal structures of the PglK mutant E510Q at resolutions ranging from 2.9Å to 5.9Å (**Fig. 2A**, **Extended Data Fig. 4 and Extended Data Table 1**). Two structures were obtained of the apo protein, revealing distinct inward-facing conformations (designated apo-inward-1 and -2), whereas the third was of ADP-bound PglK, resulting in an unprecedented, outward-occluded conformation. Given the limited resolution of X-ray data for the latter, its building was helped by the finding of Rees and colleagues[37] that transmembrane helices of ABC exporters move in pairs during structural transitions. We confirmed the register of the resulting model by collecting anomalous diffraction data of Hg-soaked crystals and a selenomethionine derivative, indicating cysteine and methionine positions (**Extended Data Fig. 5**). The fold of PglK is similar to that of other ABC exporters, first identified in the Sav1866 structure[38] (**Extended Data Fig. 6A**). However, PglK contains an additional, short α-helix (external helix "EH") at the periplasmic membrane boundary and parallel to the plane of the membrane. This novel structural motif has an essential role in LLO binding (see below).

The physiological relevance of inward-facing conformations of ABC exporters revealing large NBD separation is still under debate, because they generally reflect apo states that may only be sparsely populated *in vivo*, because nucleotides (ADP and ATP) are present at concentrations far above the relevant Kd and Km values. The structures of our apo-inward-1 and outward-occluded states were obtained from PglK protein crystallized using lauryl maltose neopentyl glycol (LMNG) as a detergent, whereas the structure of the apo-inward 2 conformation was obtained using dodecyl maltoside (DDM) (**Extended Data Table 1**). Crystal contacts in each of the three crystal forms are distinct, as are the crystallization conditions (**Extended Data Fig. 7**). This finding suggests that the type of detergent and the lattice contacts, rather than intrinsic properties or dynamics of the protein, define the degree of NBD separation of inward-facing conformations. By contrast, the NBD arrangement in our outward-occluded state resembles a "closed sandwich dimer" state observed in multiple nucleotide-bound structures of ABC transporters[24,38] or isolated ABC domains[39,40]. A comparison of the three states of PglK reveal that the main conformational changes are represented by a scissor-like movement of TM4/TM5 towards TM6, with the pair of helices moving as a rigid body and tilting by 16º (apo-inward-1 vs. apo-inward-2) and 40º (apo-inward-1 vs. outward-occluded) (**Fig. 2B** and **Extended Data Fig. 6B**). At the periplasmic surface, the outward-occluded conformation of PglK differs from the fully outward-facing structure of Sav1866[38] in that only a small opening to the central translocation pathway exists. Outward-occluded PglK thus reflects an intermediate conformation between the occluded state of the antibacterial peptide ABC exporter McjD[41] and the fully outward-open Sav1866[38] (**Extended Data Fig. 6C**).

Role of external helix in PglK-LLO interaction

The loop connecting TM1 and TM2 of PglK contains the above-mentioned external helix EH (**Fig. 2A and 3A**). Several hydrophobic, hydrophilic and cation-π interactions define the orientation of EH relative to the transmembrane domain (**Fig. 3A**). As a consequence, two hydrophobic grooves are formed near the external membrane boundary, one between each EH and TM1 and TM2 of PglK (**Fig. 3A**). Given its unusual location and surface, we investigated the functional relevance of EH by studying PglK mutants *in vivo* and *in vitro*. We generated a triple mutant of prominently located tyrosine residues in EH (Y50A/Y56A/Y63A, termed EHm1), a double mutant of positively charged residues (R53A/K55A, termed EHm2) involved in stabilizing interactions, and a deletion mutant where the entire helix (residues S46-P67) was replaced by a 8 residue-containing, flexible linker sequence (termed ΔEH). When reconstituted in liposomes, the three EH mutants showed unaltered basal ATPase activity but no stimulation

upon LLO addition, suggesting that mutating EH has uncoupled the ATPase activity of PglK from a potential binding of LLO (**Fig. 3B**). In detergent, the basal ATPase levels of the two EH mutants EHm1 and EHm2 were higher than that of WT, whereas that of ΔEH was slightly lower. Importantly, however, ATPase stimulation by LLO was absent in detergent as it was in liposomes. In agreement with the lack of LLO-stimulated ATPase activity, the *in vitro* flipping rate of the ΔEH mutant was too low to be accurately determined, whereas the flipping rates of EHm1 and EHm2 were found to be between 15– and 33–fold lower than WT (**Fig. 3C, Extended Data Fig. 3A**). Furthermore, ΔEH had completely lost *in vivo* activity, whereas the multi-alanine mutants EHm1 and EHm2 resulted only in a slightly lower *in vivo* output activity compared to WT (**Fig. 3D**). It is important to note that reductions of the *in vivo* output of the biosynthetic glycosylation pathway as a consequence of a PglK mutation may not directly correlate to the reduction of the *in vitro* flipping rate, because the rate-limiting steps of the *in vivo* glycosylation pathway are unknown. A similar phenomenon has previously been observed for *in vivo* studies of PglB mutants that exhibit reductions of *in vitro* glycosylation rates of >2 orders of magnitude, while the *in vivo* output of the same mutant was only marginally affected[22,28,32,33].

We speculated that the hydrophobic grooves formed near EH at the membrane boundary of PglK might contribute to LLO binding (**Fig. 3A**). Such an interaction could favor the positioning of the pyrophosphate moiety of LLO for entering the translocation cavity and thus initiate the flipping reaction. Because no direct structure of bound LLO could be obtained, we investigated PglK activity using synthetic compounds representing structurally truncated versions of native LLO (**Fig. 3E, Extended Data Fig. 1**). Intriguingly, none of the truncated LLOs stimulated the ATPase activity of PglK when reconstituted in proteoliposomes, suggesting that their shorter polyprenyl tails (maximum of 20 carbon atoms in geranyl-geranyl-PP-GlcNac) may prevent the simultaneous recognition of the polyprenyl and pyrophosphate groups by PglK in a lipid bilayer (**Extended Data Fig. 8**). In contrast, we observed ATPase stimulation of PglK in detergent by farnesyl-pyrophosphate (FPP), which does not contain any carbohydrate moiety, but also by farnesyl-PP-GlcNAc and geranyl-geranyl-PP-GlcNac. Unlike in lipid bilayers, the stimulation of the ATPase activity of PglK in detergent may be due to the binding of multiple truncated LLO molecules. Notably, we found that ubiquinone, a molecule with a similar polyprenyl tail as native LLO (C50), but a distinct head-group (**Fig. 3E and Extended Data Fig. 1**), did not stimulate the ATPase activity of PglK, neither in detergent nor in liposomes, suggesting that interactions both with the polyprenyl tail of LLO and the pyrophosphate moiety are essential for a productive, ATPase-stimulating interaction with PglK. When using native LLO, we found

positive cooperativity of ATPase stimulation by LLO (Km_{LLO} = 8.2 ± 0.8 μM; h_{Hill} = 1.9 ± 0.4, **Extended Data Fig. 3C**), which correlates with the presence of two regions on the surface of PglK that can interact with LLO molecules. From the above experiments we conclude that the newly identified EH has a role in mediating productive interaction of the polyprenyl tail of LLO with PglK. It is unclear at present whether this is achieved through direct binding or through a potential allosteric interaction.

.

Function of inward- and outward-facing cavities

The inward-facing PglK structures revealed a large cavity that is accessible to the cytoplasmic side and the inner leaflet of the bilayer (**Fig. 4A**). Analogous cavities have been observed in apo-inward-facing structures of other ABC transporters[24,35,42], where they have been interpreted to reflect substrate-binding pockets. Analogous to the proposal of Lipid–A flipping by MsbA[24], one might speculate that LLO flipping by PglK requires the polyprenyl (C55) tail to enter an inward-facing cavity through the side entrance open to the lipid bilayer. However, not only would this require the apo-inward conformation of PglK to be a predominant state in the membrane (which appears highly unlikely given cellular nucleotide concentrations), but such a reaction would also contradict the essential nature of the external helix EH shown above. In addition, the polyprenyl tail would have to fold (essentially "curl up") into the very bottom of the cavity, the only place where the surface of the cavity is hydrophobic (**Fig. 4A and Extended Data Fig. 6D**). We nevertheless tested this hypothesis and reduced the volume of the hydrophobic section of the inward-facing cavity by ~60%[43] by introducing four bulky residues, two in each PglK subunit (S294F/V297W). The resulting mutant retained wild type *in vivo* and *in vitro* flipping rates and unaltered ATPase stimulation (**Fig. 4C-E**), strongly arguing against the involvement of this cavity in polyprenyl binding and suggesting that the polyprenyl moiety remains exposed to the lipid bilayer during flipping.

Could the pyrophosphate-oligosaccharide head-group be accepted into to the inward-facing cavity during flipping? This seems highly unlikely for the following reason: As a consequence of the domain-swapped architecture of ABC exporters, TM4-TM5 of each PglK subunit cross over and bind the NBD of the opposite subunit. The cavity formed by the inward-facing state is thus defined by the separation of TM4 and TM6 (**Fig. 2B**). If the head-group of LLO were to enter this cavity, the LLO molecule would be "pinched off" in the middle during the transition of PglK to outward-facing, as the gap between TM4 and TM6 closes and a distinct gap (between TM1 and TM3) opens to the outside. This would essentially trap the LLO molecule and produce a

massive steric clash, preventing substrate release. The above considerations lead to the inevitable conclusion that during the flipping cycle of PglK, the inward-facing cavity does not contribute to LLO binding.

In contrast, the central cavity of PglK in the outward-occluded conformation is distinct in chemical nature from that of the inward-facing conformation. We also modeled a fully outward-facing state of PglK based on the structure of Sav1866[38], exploiting the finding of Rees and colleagues[37] that transmembrane helices move in pairs (TM1/2, TM3/6, TM4/5) when ABC exporters change conformations. The resulting homology model of outward-open PglK features a similar cavity as our outward-occluded structure, but with a wider opening to the periplasmic side of the membrane (**Fig. 4A,B**). The outward-facing cavity spans almost the entire membrane bilayer, and whereas our outward-occluded structure provides too little space to harbor the LLO head-group (i.e. the pyrophosphate moiety and the saccharides), the fully outward-facing conformation would provide sufficient space. Intriguingly, we identified a belt of positively charged residues (R86, R260, R302 and R309) lining the interior of the outward-facing cavity, accounting for a total of 8 positive charges (**Fig. 4B**). Due to the scissoring motion required to convert ABC exporters from inward- to outward-facing, these arginines are buried and/or forming salt-bridges in the inward-facing conformations and only become accessible when PglK is in an outward-facing or outward-occluded states. Because the arginines might serve as binding partners of the pyrophosphate moiety of LLO, we generated individual alanine mutants (R86A, R260A, R302A, R309A) and a fourfold mutant with all 8 charges removed. While each individual alanine mutant maintained flipping activity both *in vivo* and *in vitro*, the fourfold mutant had completely lost activity (**Fig. 4D-E**). At the same time, while each individual mutant retained stimulation of ATPase activity (albeit with a lower basal ATPase rate), the ATPase activity of the fourfold mutant was no longer stimulated by LLO (**Fig. 4C**), suggesting an apparent loss of interaction between LLO and mutant PglK.

Flipping mechanism

The accumulated biochemical and structural evidence allow us to propose the flipping mechanism shown in **Fig. 5**. The two conformations of PglK that are relevant for LLO flipping are outward-occluded (ADP-bound) and outward-facing (ATP-bound). Given the constant presence of ADP and ATP in the cell, an apo-state of the transporter, represented by an inward-facing conformation, is probably transient and sparsely populated. It is conceivable that fast exchange of ATP for ADP would never allow the two ATP binding sites of the homodimeric

PglK protein to be nucleotide-free at the same time. We propose that the surface of PglK including and around EH provides an attachment point for the polyprenyl tail, whereas the pyrophosphate moiety is attracted into the outward-facing conformation of the ATP-bound state through electrostatic interactions provided by the arginine residues exposed in the outward-facing cavity. The oligosaccharide follows the pyrophosphate but does not require any specific interactions, explaining the low selectivity of the translocation reaction with respect to the type and number of saccharides. This is not only consistent with the observation that PglK can flip LLO involved in O-antigen assembly, normally transported by the MOP-type flippase Wzx[21], but can also explain how related ABC-type flippases can translocate long, linear polysaccharides in O-antigen generation[44]. In the latter, the elongated oligosaccharide can be imagined to slide into an outward-facing translocation pathway from the cytoplasmic side and leave on the external side, while the pyrophosphate moiety is the essential component recognized and bound by the protein. The driving force of the flipping reaction of PglK is probably two-fold: First, as hydrolysis of ATP pushes the NBDs apart for product release, transmission of this motion to the TMDs causes lateral pressure to be exerted on the enclosed substrate. This is reminiscent of the peristaltic component proposed for the mechanism of the vitamin B12 ABC importer[45]. Second, once LLO has left the translocation pathway PglK will adopt an outward-occluded conformation, as demonstrated in our ADP-bound structure, thereby effectively closing the door behind the bulky oligosaccharide. We conclude that the energy gained by the hydrolysis of ATP is used to break the interaction of the pyrophosphate moiety with the essential arginines lining the outward-facing cavity of PglK. It is conceivable that pyrophosphate-containing LLO accumulated on the periplasmic side might act as an inhibitor of the flipping reaction, consistent with the slowing of the flipping rate in our *in vitro* assay. *In vivo*, a similar problem might occur if the undecaprenyl-pyrophosphate were to be accumulated after transfer of the glycan by PglB[22], but may be avoided by the quick hydrolysis of undecaprenyl-pyrophosphate to the monophosphate species[23] (**Extended Data Fig. 2**).

The LLO flipping mechanism we deduced for PglK has a resemblance to the "credit card swipe" model proposed for the flipping of phospholipids by P4-ATPases flippases[46-48]. Two key differences are the proposed firm attachment of the polyprenyl tail to the PglK surface by means of EH, and the requirement of a long, sufficiently wide translocation pathway that harbors the pyrophosphate and oligosaccharide moieties during flipping. Our mechanism is distinct from a proposed model of MsbA mechanism, which suggested that the entire lipid-A core may enter the inward-facing, nucleotide-free state of the transporter[24], and also distinct from the canonical

alternating-access model used to explain the mechanism of transporters of small, hydrophilic substrates.

Conclusions

Our results define the structural and mechanistic basis of lipid-linked oligosaccharide flipping by an ABC transporter. The data suggest a flipping mechanism suitable for the translocation of a large head-group containing a pyrophosphate moiety and a linear polysaccharide, both of which are shielded from the lipid bilayer in a translocation cavity. We envision that the proposed, direct jump into the outward-facing conformation and the putative interaction of the lipid tail with the membrane-facing surface of the transporter may be a feature of other ABC-type LLO flippases and possibly of MOP-type transporters involved in bacterial cell wall assembly or responsible for N-glycan flipping in eukaryotes[16,21]. Understanding the molecular mechanism of LLO flipping may open new ways to modify the glycosylation machinery in bacteria, which could be exploited for the generation of novel glyco-conjugates or glyco-proteins that may have applications in diagnosis or therapeutics[49,50].

Methods summary

Structural studies: *Campylobacter jejuni* PglK containing a N-terminal His_{10} affinity tag was expressed in *E. coli* cells and purified in lauryl maltose neopentyl glycol. PglK was crystallized in the presence or absence of ADP. For experimental phasing, crystals were soaked in ethyl mercury phosphate (EMP) before data collection. The phase problem was solved by MIRAS for the apo-inward-1 structure and molecular replacement for the apo-inward-2 and outward-occluded structures, using a partial model from the apo-inward-1 structure as a search model. SAD experiments on crystals from a selenomethionine derivative confirmed the polypeptide chain register of the outward-occluded structure.

In vitro activity assays: Isolation of LLOs (native and tLLO) from *E. coli* SCM6 cells carrying mutated *C. jejuni pgl* clusters for LLO biosynthesis was performed as described previously[32]. For *in vitro* flipping, PglK- and tLLO-containing proteoliposomes were incubated with 5mM $MgCl_2$ and ATP. To stop the flipping reaction, samples were diluted into a buffer containing 4mM ADP. Labeling of non-flipped tLLO was achieved by incubation with purified glycosyltransferase PglH in the presence of 50µM [^{3}H]-UDP-GalNAc. ATPase activities were determined as described previously[45].

In vivo flipping assays: PglK was expressed in *E. coli* SCM6[22] cells carrying the *Campylobacter jejuni pgl* cluster (containing an inactivated *pglK* gene)[19], and a single-chain variable antibody fragment containing the glycosylation sequon DQNAT[51]. Glycosylation of 3D5 was analyzed by immunoblot with anti-glycan serum hR6[28].

Synthesis of LLO analogs: Farnesyl- and geranylgeranyl-PP-GlcNAc were synthesized in seven steps from commercially available lipids and sugar following an established procedure[52]. The two LLOs were obtained as pure compounds and were fully characterized.

Figure Legends

Figure 1. Biochemical characterization of PglK. (A) Schematic of *in vitro* LLO flipping assay. Proteoliposomes contain PglK homodimer (subunits in orange and gray) and tLLO, both in 50_{in}:50_{out} orientations (see Methods and **Extended Data Fig. 10**). Due to external addition of ATP, only inside-out transporters catalyze tLLO flipping. The undecaprenyl tail of tLLO is shown in purple; *Red hexagon*, di-N-acetylbacillosamine; *yellow square*, N-acetylgalactosamine; *yellow square with asterisks*, [^{3}H] N-acetylgalactosamine. PglK activity is inhibited by addition of excess ADP, upon which proteoliposomes are incubated with purified PglH and [^{3}H] UDP-GalNAc to label and quantitate tLLO remaining in the external leaflet. (B) tLLO flipping of wild type (WT) PglK and E510Q mutant. +ADP, assay in the presence of 4mM ADP. –ATP, assay in the absence of ATP. liposomes, empty liposomes containing only tLLO. (C) *In vitro* tLLO flipping of PglK WT (as in panel B) and E510Q mutant (see also **Extended Data Fig. 3A**). Bars indicate initial velocities. (D) *In vivo* LLO flipping of wild type PglK and E510Q mutant expressed in *E.coli* SCM6 cells containing the *C. jejuni pgl* operon[32]. E.V., empty vector, N.I.C., non-induced cells. Anti-glycan refers to HR6 antibody recognizing the N-glycan of a substrate protein (see Methods), whereas anti-PglK is used to monitor PglK expression level. (E) Determination of Km values of ATP hydrolysis and ATP-driven *in vitro* tLLO flipping. Cpm, counts per million. (F) ATPase activity in the presence (+) or absence (-) of native LLO of wild type (WT) PglK and E510Q mutant in detergent (LMNG) or proteoliposomes. (G) ATPase activity of PglK in detergent in the presence of LLO (20μM), tLLO (20μM), diverse drugs (50μM), and Lipid A (20μM). For details see Methods. Error bars, s.d. (n = 3).

Figure 2. (A) PglK structures in inward- and outward-facing states, with subunits in orange and grey. EH, external α-helix. (B) Structural conversion from inward- to outward-facing conformations. A single PglK subunit is shown in light orange, with TM4, TM5, and TM6 shown in ribbon representation. TM4-6 of a superimposed PglK subunit in the apo-inward-1 state (light yellow) or the outward-facing homology model (dark orange) are shown as ribbons to illustrate conformational changes converting the different states. ICL, intracellular loop.

Figure 3. Structural and biochemical characterization of the external helix (EH). (A) *Left*; Hydrophobic groove (green) formed by EH at the interface PglK-membrane. *Right*; Close-up of EH with prominently placed residues indicated. (B) ATPase activity in the presence (+) or absence (–) of LLO of PglK WT and variants in detergent (LMNG) or proteoliposomes. (C) *In*

vitro tLLO flipping of PglK WT and mutants. Bars indicate initial velocities. (D) *In vivo* LLO flipping study of PglK WT and variants expressed in *E.coli* SCM6 cells. (E) ATPase activity of PglK in detergent or proteoliposomes in the presence of diverse lipids and glycolipids; Geranylgeranyl-PP-GlcNAc (GGPPGlcNAc) (90µM), farnesyl-PP-GlcNAc (FPPGlcNAc) (90µM), farnesyl-PP (FPP) (90µM), Ubiquinone (90µM). ΔEH, GSSGSSGS linker. EHm1, Y50A/Y56A/Y63A. EHm2, R53A/K55A. Error bars, s.d. (n = 3).

Figure 4. Analysis of translocation pathway of PglK. (A) Comparison of cavities (green) in inward-facing and outward-occluded states, with native LLO shown as space-filling model for size reference. (B) Side view of fully outward-facing homology model of PglK based on Sav1866 structure[38]. Cavity-exposed, positively charged side chains are shown as blue sticks and labeled. (C) ATPase activity of WT PglK and mutants in detergent (LMNG) and proteoliposomes, in the presence (+) or absence (-) of native LLO. (D) *In vitro* tLLO flipping of PglK WT and variants. Bars indicate initial velocities. (E) *In vivo* LLO flipping of PglK WT and variants expressed in *E.coli* SCM6 cells. Tetra, R86A/R260A/R302A/R309A. Error bars, s.d. (n = 3).

Figure 5. Proposed LLO flipping mechanism. PglK is shown as cylinder model with subunits colored grey and orange. EH, red. Relevant positively charged side chains are shown as blue sticks and labeled. State 5 reflects inward-facing structure apo-inward-1, states 1 and 4 reflect outward-occluded structures, states 2 and 3 reflect outward-open conformations (modeled based on the Sav1866 structure[38]). The proposed molecular events indicated by arrows are: a, polyprenyl tail of LLO interacting with the PglK region including and around EH, exchanging ADP for ATP; b, pyrophosphate-oligosaccharide head-group entering outward-facing cavity; c, ATP hydrolysis, LLO head-group release on external side of the membrane, inorganic phosphate release; d, polyprenyl tail disengagement; e, PglK futile ATPase cycle. The polyprenyl tail of LLO is shown in purple. *Red hexagon*, di-N-acetylbacillosamine; *yellow square*, N-acetylgalactosamine; *blue circle*, glucose.

Extended Data Fig. 1. Structures of lipid-linked-oligosaccharides and chemical analogs used in this study.

Extended Data Fig. 2. LLO synthesis and N-glycosylation in *Campylobacter jejuni*. *Red hexagon*, di-N-acetylbacillosamine; *yellow square*, N-acetylgalactosamine; *blue circle*, glucose. The LLO polyprenyl tail is shown in purple. A periplasmic polypeptide chain is shown in blue. PglH (red) is the glycosyltransferace used in the *in vitro* tLLO flipping assays. Und-PP-ase, undecaprenyl pyrophosphatase.

Extended Data Fig. 3. (A) *In vitro* tLLO flipping of PglK mutants E510Q, EHm1 and EHm2. +ADP, assay in the presence of 4mM ADP. –ATP, assay in the absence of ATP. liposomes, empty liposomes containing only tLLO. ADP alone does not cause tLLO to disappear from the external liposomes leaflet. (B) Determination of Km values of ATP hydrolysis in the presence (+) or absence (-) of LLO (20μM). Stimulation results in higher V_{max}, while the K_m for ATP remains almost unaltered in the presence ($Km_{(+LLO)}$ = 0.54 ± 0.03 mM) or absence ($Km_{(-LLO)}$ = 0.36 ± 0.04 mM) of native LLO. (C) Determination of Km value of ATPase stimulation by native LLO in detergent (rates are normalized against the basal activity in absence of LLO).

Extended Data Fig. 4. (A) and (B), Stereo views (cross-eyed) of the 2Fo-Fc electron density maps for the complete PglK dimer of the structures at 2.9 and 3.9Å, respectively. (C) Stereo view of the NCS averaged electron density map for the complete PglK dimer of the structure at 5.9Å and close-up of the NBDs showing the Fo-Fc electron density map for the bound ADP molecules. 2Fo-Fc and NCS maps are shown at 1.0 sigma level. Fo-Fc maps are shown at 3.0 sigma level.

Extended Data Fig. 5. Validation of side chain register of outward-occluded PglK model. Anomalous electron density maps (A, B and C) define selenomethionine, cysteine-bound mercury and $PtCl_4$ sites, respectively. Contour levels are between 4.0 to 5.0σ. In (A) Anomalous density was observed for 9 of 10 selenomethionines of PglK.

Extended Data Fig. 6. (A) Ribbon diagram of one PglK subunit depicting the secondary structure arrangement, based on the Sav1866 nomenclature[38]. ICL, intracellular loop. EH, external helix (B) Conformational changes of TM4 and TM5 visualized after superposition of subunits of apo-inward-1 (light orange) and apo-inward-2 structures (dark orange). (C) Structures of the antibacterial peptide ABC exporter McjD in occluded state (PDB code 4PLO), PglK in outward-occluded state, and the ABC exporter Sav1866 (PDB code 2HYD) in outward-open state. Transmembrane helices TM1 and TM3 (purple) define the extent of the external

opening. Subunits in each dimer are shown in orange and gray. (D) Side and cytoplasmic view cutoff of PglK apo-inward-1 structure and vacuum electrostatic surface representation showing the internal cavity.

Extended Data Fig. 7. PglK crystal packing. (A), (B), and (C) show the main crystal contacts of apo-inward-1 (2.9Å resolution), apo-inward-2 (3.9Å resolution), and outward-occluded (5.9Å resolution) states, respectively.

Extended Data Fig. 8. Putative interactions of native LLO (A) and synthetic LLO analogs (B) with PglK in apo-inward and outward-occluded states. *Red hexagon*, di-N-acetylbacillosamine; *yellow square*, N-acetylgalactosamine; *blue circle*, glucose; *blue square*, N-acetylglucosamine. The LLO polyprenyl tail is shown in purple.

Extended Data Fig. 9. (A) Product analysis of tLLO glycosylation catalyzed by PglH. The reaction products were analyzed by *in vitro* glycosylation of a fluorescently labeled substrate peptide (DQNAT sequon) catalyzed by PglB as reported earlier[32,33]. Depending on the presence and size of the N-glycan, peptides show a different mobility after Tricine SDS–PAGE. Bands were visualized using a fluorescence gel scan (488 nm excitation and 526 nm emission). Lane 1; product of the deglycosylation reaction of hexasaccharide LLO catalyzed by α-N-Acetylgalactosaminidase, which removes terminal GalNAc molecules. This demonstrates the purity of the LLO used with respect to GalNAc. Lane 2; tLLO used in biochemical assays. Lane 3; products of tLLO glycosylation when tLLO:GalNAc molar ratio is 2:1. Lane 4; products of tLLO glycosylation when tLLO:GalNAc molar ratio is 1:1. Lane 5; products of tLLO glycosylation when tLLO:GalNAc molar ratio is 1:10. *Red hexagon*, di-N-acetylbacillosamine; *yellow square*, N-acetylgalactosamine. (B) PglK proteoliposomes incubated in the presence of 4mM ADP. The level of tLLO in the external leaflet after t = 40' remains unchanged (104.2 +/- 10.8%) relative to the amount at t = 0. ADP alone does not cause a decrease in the concentration of tLLO in the external liposomes leaflet, ruling out a potential sequestration of tLLO in the outward-occludded state of PglK.

Extended Data Fig. 10. (A) Determination of tLLO orientation in proteoliposomes. Disrupted liposomes (0.3% Triton-X100) and non-disrupted proteoliposomes were incubated with PglH in the presence of excess GalNAc. The amount of glycopeptide was determined from band intensities of fluorescence gel scans. 48.2 +/- 7.5 % of tLLO is located in the outer leaflet of the

bilayer. *Red hexagon*, di-N-acetylbacillosamine; *yellow square*, N-acetylgalactosamine. (B) Determination of PglK orientation in proteoliposomes. The fully functional mutant PglK-(C269L/C352S/C386S/C549L/S544C) was reconstituted in proteoliposomes and labeled with negatively charged Alexa Fluor® 488 C5 Maleimide. The fluorescence of non-disrupted and disrupted proteoliposomes was compared. 51.8 +/- 2.8 % of the PglK molecules are oriented with NBDs facing outwards.

Acknowledgements: We gratefully acknowledge the assistance of staff scientists at the PX beamline of the Swiss Light Source, Villigen, Switzerland. We thank Maja Napiorkowska and Ana Ramirez for assistance with the PglB assays. This work was supported by the Swiss National Science Foundation (SNF 31003A–146191 to K.P.L. and Transglyco Sinergia program to M.A., J.-L.R., and K.P.L.). C.P. acknowledges support from the ETH postdoctoral fellowship program.

Author Contributions

C.P. determined the structures of PglK, established the *in vitro* flipping assay, and performed *in vivo* flipping studies. S.G. crystallized PglK in apo-inward 2 state, M.B. assisted in expression and purification of PglK. J.B., T.D., and J.-L.R. synthesized LLO analogs. K.P.L., S.G., M.A., and C.P. conceived the project. K.P.L., M.A., and C.P. analyzed the data. K.P.L. and C.P. wrote the manuscript, all authors contributed to manuscript revision.

References

1. Burda, P. & Aebi, M. The dolichol pathway of N-linked glycosylation. *Biochim Biophys Acta* **1426**, 239-57 (1999).
2. Helenius, J. et al. Translocation of lipid-linked oligosaccharides across the ER membrane requires Rft1 protein. *Nature* **415**, 447-50 (2002).
3. Sprong, H., van der Sluijs, P. & van Meer, G. How proteins move lipids and lipids move proteins. *Nat Rev Mol Cell Biol* **2**, 504-13 (2001).
4. Sebastian, T.T., Baldridge, R.D., Xu, P. & Graham, T.R. Phospholipid flippases: building asymmetric membranes and transport vesicles. *Biochim Biophys Acta* **1821**, 1068-77 (2012).
5. Ewers, H. & Helenius, A. Lipid-mediated endocytosis. *Cold Spring Harb Perspect Biol* **3**, a004721 (2011).
6. Hankins, H.M., Baldridge, R.D., Xu, P. & Graham, T.R. Role of flippases, scramblases and transfer proteins in phosphatidylserine subcellular distribution. *Traffic* **16**, 35-47 (2015).
7. Bevers, E.M., Comfurius, P. & Zwaal, R.F. Changes in membrane phospholipid distribution during platelet activation. *Biochim Biophys Acta* **736**, 57-66 (1983).
8. Krahling, S., Callahan, M.K., Williamson, P. & Schlegel, R.A. Exposure of phosphatidylserine is a general feature in the phagocytosis of apoptotic lymphocytes by macrophages. *Cell Death Differ* **6**, 183-9 (1999).
9. Balasubramanian, K. & Schroit, A.J. Aminophospholipid asymmetry: A matter of life and death. *Annu Rev Physiol* **65**, 701-34 (2003).
10. Cuthbertson, L., Kos, V. & Whitfield, C. ABC transporters involved in export of cell surface glycoconjugates. *Microbiol Mol Biol Rev* **74**, 341-62 (2010).
11. Cuthbertson, L., Kimber, M.S. & Whitfield, C. Substrate binding by a bacterial ABC transporter involved in polysaccharide export. *Proc Natl Acad Sci U S A* **104**, 19529-34 (2007).
12. Clarke, B.R., Cuthbertson, L. & Whitfield, C. Nonreducing terminal modifications determine the chain length of polymannose O antigens of Escherichia coli and couple chain termination to polymer export via an ATP-binding cassette transporter. *J Biol Chem* **279**, 35709-18 (2004).
13. Sharom, F.J. Flipping and flopping--lipids on the move. *IUBMB Life* **63**, 736-46 (2011).
14. Kodigepalli, K.M., Bowers, K., Sharp, A. & Nanjundan, M. Roles and regulation of phospholipid scramblases. *FEBS Lett* **589**, 3-14 (2015).
15. Brunner, J.D., Lim, N.K., Schenck, S., Duerst, A. & Dutzler, R. X-ray structure of a calcium-activated TMEM16 lipid scramblase. *Nature* **516**, 207-12 (2014).
16. Hvorup, R.N. et al. The multidrug/oligosaccharidyl-lipid/polysaccharide (MOP) exporter superfamily. *Eur J Biochem* **270**, 799-813 (2003).
17. Lopez-Marques, R.L., Theorin, L., Palmgren, M.G. & Pomorski, T.G. P4-ATPases: lipid flippases in cell membranes. *Pflugers Arch* **466**, 1227-40 (2014).
18. Eckford, P.D. & Sharom, F.J. The reconstituted Escherichia coli MsbA protein displays lipid flippase activity. *Biochem J* **429**, 195-203 (2010).
19. Wacker, M. et al. N-linked glycosylation in Campylobacter jejuni and its functional transfer into E. coli. *Science* **298**, 1790-3 (2002).
20. Young, N.M. et al. Structure of the N-linked glycan present on multiple glycoproteins in the Gram-negative bacterium, Campylobacter jejuni. *J Biol Chem* **277**, 42530-9 (2002).
21. Alaimo, C. et al. Two distinct but interchangeable mechanisms for flipping of lipid-linked oligosaccharides. *EMBO J* **25**, 967-76 (2006).
22. Lizak, C., Gerber, S., Numao, S., Aebi, M. & Locher, K.P. X-ray structure of a bacterial oligosaccharyltransferase. *Nature* **474**, 350-5 (2011).
23. Tatar, L.D., Marolda, C.L., Polischuk, A.N., van Leeuwen, D. & Valvano, M.A. An Escherichia coli undecaprenyl-pyrophosphate phosphatase implicated in undecaprenyl phosphate recycling. *Microbiology* **153**, 2518-29 (2007).
24. Ward, A., Reyes, C.L., Yu, J., Roth, C.B. & Chang, G. Flexibility in the ABC transporter MsbA: Alternating access with a twist. *Proc Natl Acad Sci U S A* **104**, 19005-10 (2007).
25. Sanyal, S. & Menon, A.K. Specific transbilayer translocation of dolichol-linked oligosaccharides by an endoplasmic reticulum flippase. *Proc Natl Acad Sci U S A* **106**, 767-72 (2009).
26. Sanyal, S. & Menon, A.K. Stereoselective transbilayer translocation of mannosyl phosphoryl dolichol by an endoplasmic reticulum flippase. *Proc Natl Acad Sci U S A* **107**, 11289-94 (2010).

27. Linton, D. et al. Functional analysis of the Campylobacter jejuni N-linked protein glycosylation pathway. *Mol Microbiol* **55**, 1695-703 (2005).
28. Lizak, C. et al. A catalytically essential motif in external loop 5 of the bacterial oligosaccharyltransferase PglB. *J Biol Chem* **289**, 735-46 (2014).
29. Troutman, J.M. & Imperiali, B. Campylobacter jejuni PglH is a single active site processive polymerase that utilizes product inhibition to limit sequential glycosyl transfer reactions. *Biochemistry* **48**, 2807-16 (2009).
30. Abeijon, C. & Hirschberg, C.B. Topography of initiation of N-glycosylation reactions. *J Biol Chem* **265**, 14691-5 (1990).
31. Hanover, J.A. & Lennarz, W.J. The topological orientation of N,N'-diacetylchitobiosylpyrophosphoryldolichol in artificial and natural membranes. *J Biol Chem* **254**, 9237-46 (1979).
32. Gerber, S. et al. Mechanism of bacterial oligosaccharyltransferase: in vitro quantification of sequon binding and catalysis. *J Biol Chem* **288**, 8849-61 (2013).
33. Lizak, C. et al. Unexpected reactivity and mechanism of carboxamide activation in bacterial N-linked protein glycosylation. *Nat Commun* **4**, 2627 (2013).
34. Siarheyeva, A. & Sharom, F.J. The ABC transporter MsbA interacts with lipid A and amphipathic drugs at different sites. *Biochem J* **419**, 317-28 (2009).
35. Jin, M.S., Oldham, M.L., Zhang, Q. & Chen, J. Crystal structure of the multidrug transporter P-glycoprotein from Caenorhabditis elegans. *Nature* **490**, 566-9 (2012).
36. Raetz, C.R., Reynolds, C.M., Trent, M.S. & Bishop, R.E. Lipid A modification systems in gram-negative bacteria. *Annu Rev Biochem* **76**, 295-329 (2007).
37. Lee, J.Y., Yang, J.G., Zhitnitsky, D., Lewinson, O. & Rees, D.C. Structural basis for heavy metal detoxification by an Atm1-type ABC exporter. *Science* **343**, 1133-6 (2014).
38. Dawson, R.J. & Locher, K.P. Structure of a bacterial multidrug ABC transporter. *Nature* **443**, 180-5 (2006).
39. Zaitseva, J. et al. A structural analysis of asymmetry required for catalytic activity of an ABC-ATPase domain dimer. *EMBO J* **25**, 3432-43 (2006).
40. Smith, P.C. et al. ATP binding to the motor domain from an ABC transporter drives formation of a nucleotide sandwich dimer. *Mol Cell* **10**, 139-49 (2002).
41. Choudhury, H.G. et al. Structure of an antibacterial peptide ATP-binding cassette transporter in a novel outward occluded state. *Proc Natl Acad Sci U S A* **111**, 9145-50 (2014).
42. Shintre, C.A. et al. Structures of ABCB10, a human ATP-binding cassette transporter in apo- and nucleotide-bound states. *Proc Natl Acad Sci U S A* **110**, 9710-5 (2013).
43. Voss, N.R. & Gerstein, M. 3V: cavity, channel and cleft volume calculator and extractor. *Nucleic Acids Res* **38**, W555-62 (2010).
44. Whitfield, C. & Trent, M.S. Biosynthesis and export of bacterial lipopolysaccharides. *Annu Rev Biochem* **83**, 99-128 (2014).
45. Korkhov, V.M., Mireku, S.A. & Locher, K.P. Structure of AMP-PNP-bound vitamin B12 transporter BtuCD-F. *Nature* **490**, 367-72 (2012).
46. Vestergaard, A.L. et al. Critical roles of isoleucine-364 and adjacent residues in a hydrophobic gate control of phospholipid transport by the mammalian P4-ATPase ATP8A2. *Proc Natl Acad Sci U S A* **111**, E1334-43 (2014).
47. Stone, A. & Williamson, P. Outside of the box: recent news about phospholipid translocation by P4 ATPases. *J Chem Biol* **5**, 131-6 (2012).
48. Pomorski, T. & Menon, A.K. Lipid flippases and their biological functions. *Cell Mol Life Sci* **63**, 2908-21 (2006).
49. Hug, I. & Feldman, M.F. Analogies and homologies in lipopolysaccharide and glycoprotein biosynthesis in bacteria. *Glycobiology* **21**, 138-51 (2011).
50. Jones, C. Vaccines based on the cell surface carbohydrates of pathogenic bacteria. *An Acad Bras Cienc* **77**, 293-324 (2005).
51. Lizak, C., Fan, Y.Y., Weber, T.C. & Aebi, M. N-Linked glycosylation of antibody fragments in Escherichia coli. *Bioconjug Chem* **22**, 488-96 (2011).
52. Liu, F. et al. Rationally designed short polyisoprenol-linked PglB substrates for engineered polypeptide and protein N-glycosylation. *J Am Chem Soc* **136**, 566-9 (2014).

Fig. 1

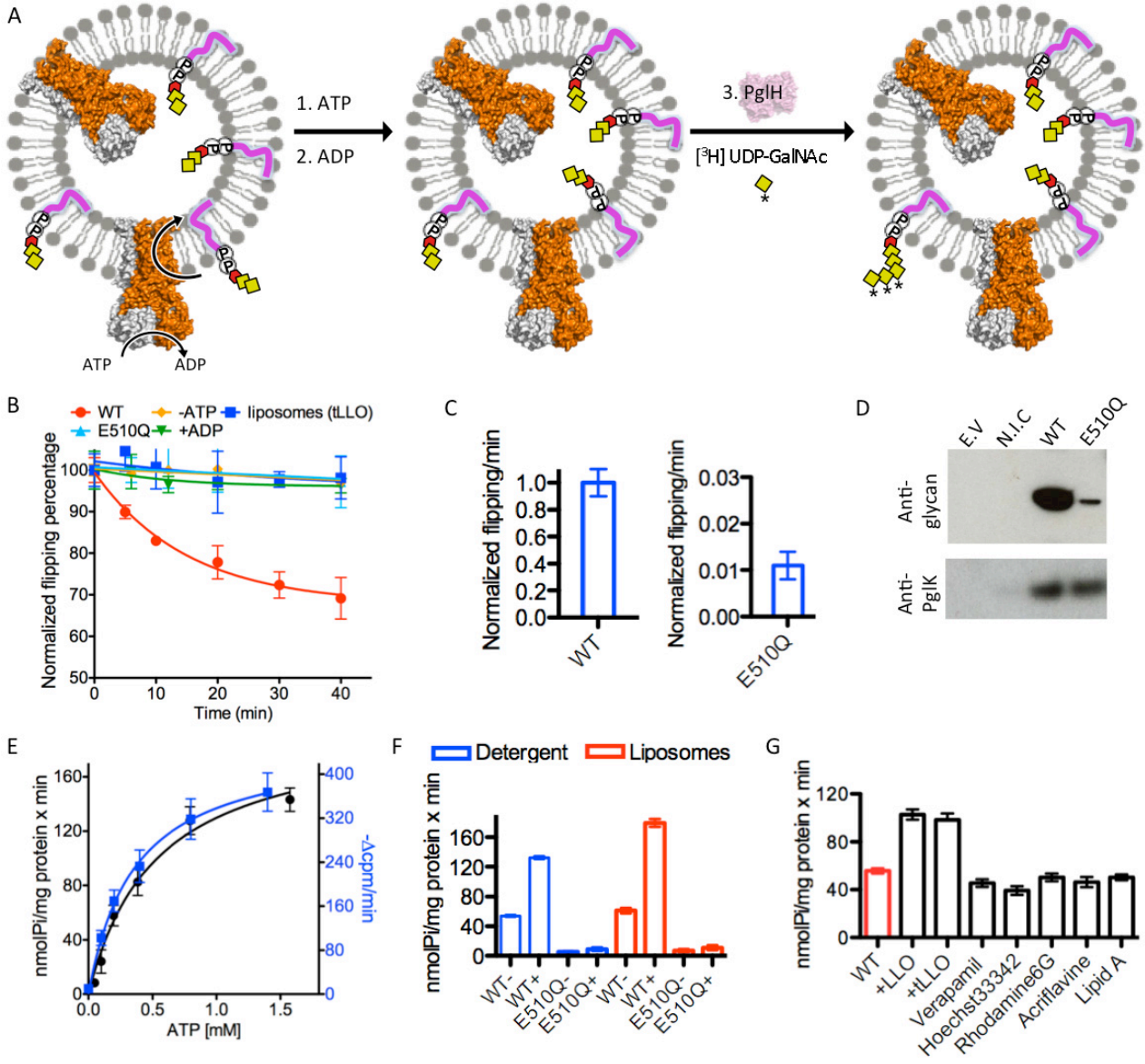
A
1. ATP
2. ADP
3. PglH
[3H] UDP-GalNAc
ATP
ADP
B
WT
E510Q
-ATP
+ADP
liposomes (tLLO)
Normalized flipping percentage
Time (min)
C
Normalized flipping/min
WT
E510Q
D
E.V
N.I.C
WT
E510Q
Anti-glycan
Anti-PglK
E
nmolPi/mg protein x min
-Δcpm/min
ATP [mM]
F
Detergent
Liposomes
nmolPi/mg protein x min
WT-
WT+
E510Q-
E510Q+
G
nmolPi/mg protein x min
WT
+LLO
+tLLO
Verapamil
Hoechst33342
Rhodamine6G
Acriflavine
Lipid A

Fig. 2

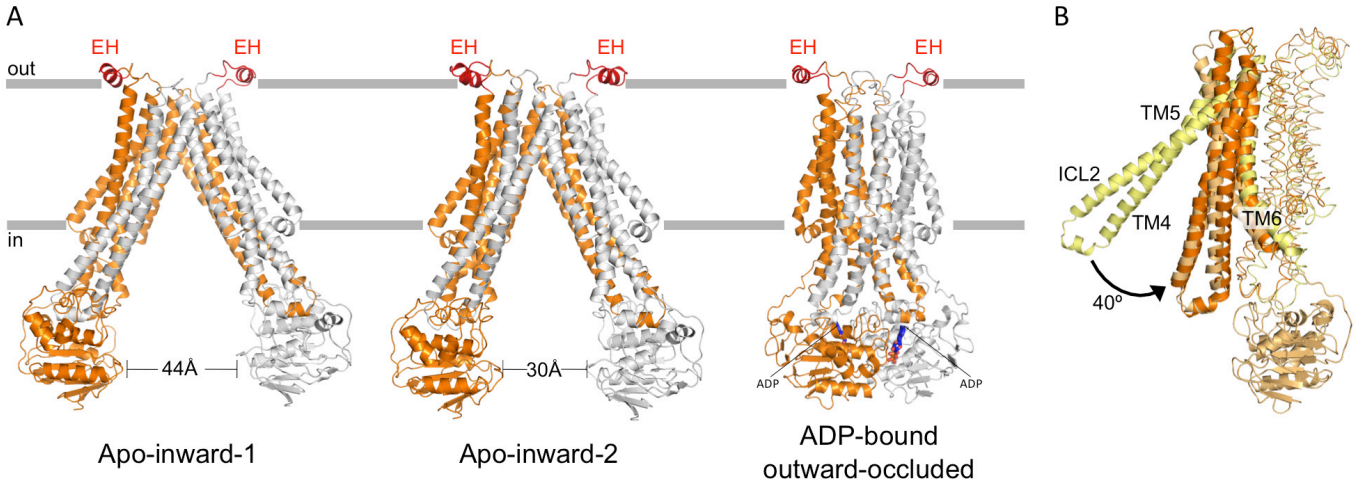
A
EH
EH
EH
EH
EH
EH
out
in
44Å
30Å
ADP
ADP
Apo-inward-1
Apo-inward-2
ADP-bound
outward-occluded
B
TM5
ICL2
TM4
TM6
40°

Fig. 3

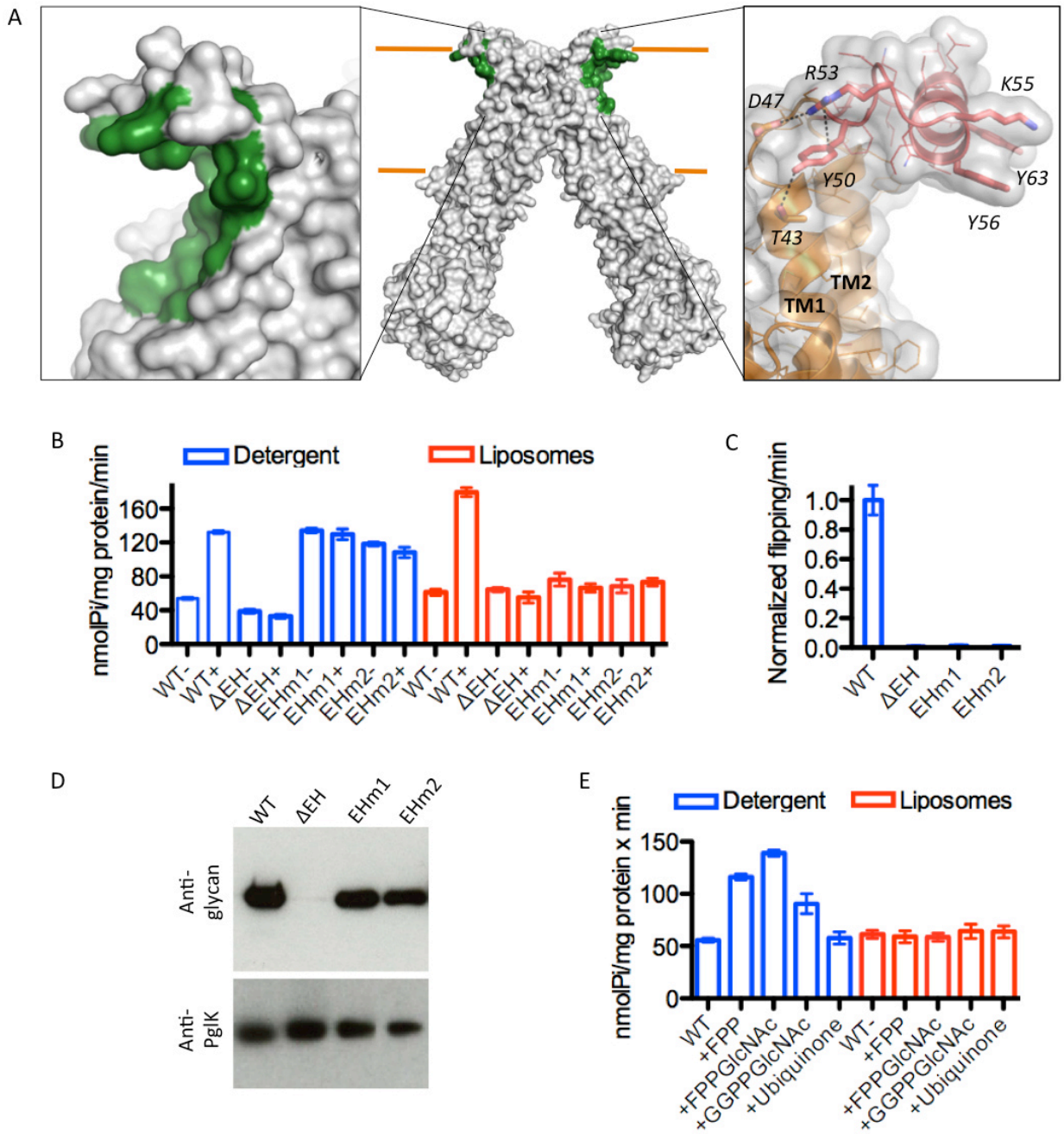
A
R53
K55
D47
Y50
Y63
Y56
T43
TM2
TM1
B
Detergent
Liposomes
nmolPi/mg protein/min
160
120
80
40
0
WT-
WT+
ΔEH-
ΔEH+
EHm1-
EHm1+
EHm2-
EHm2+
C
Normalized flipping/min
1.0
0.8
0.6
0.4
0.2
0.0
WT
ΔEH
EHm1
EHm2
D
WT
ΔEH
EHm1
EHm2
Anti-glycan
Anti-PglK
E
Detergent
Liposomes
nmolPi/mg protein x min
150
100
50
0
WT
+FPP
+FPPGlcNAc
+GGPPGlcNAc
+Ubiquinone
WT-
+FPP
+FPPGlcNAc
+GGPPGlcNAc
+Ubiquinone

Fig. 4

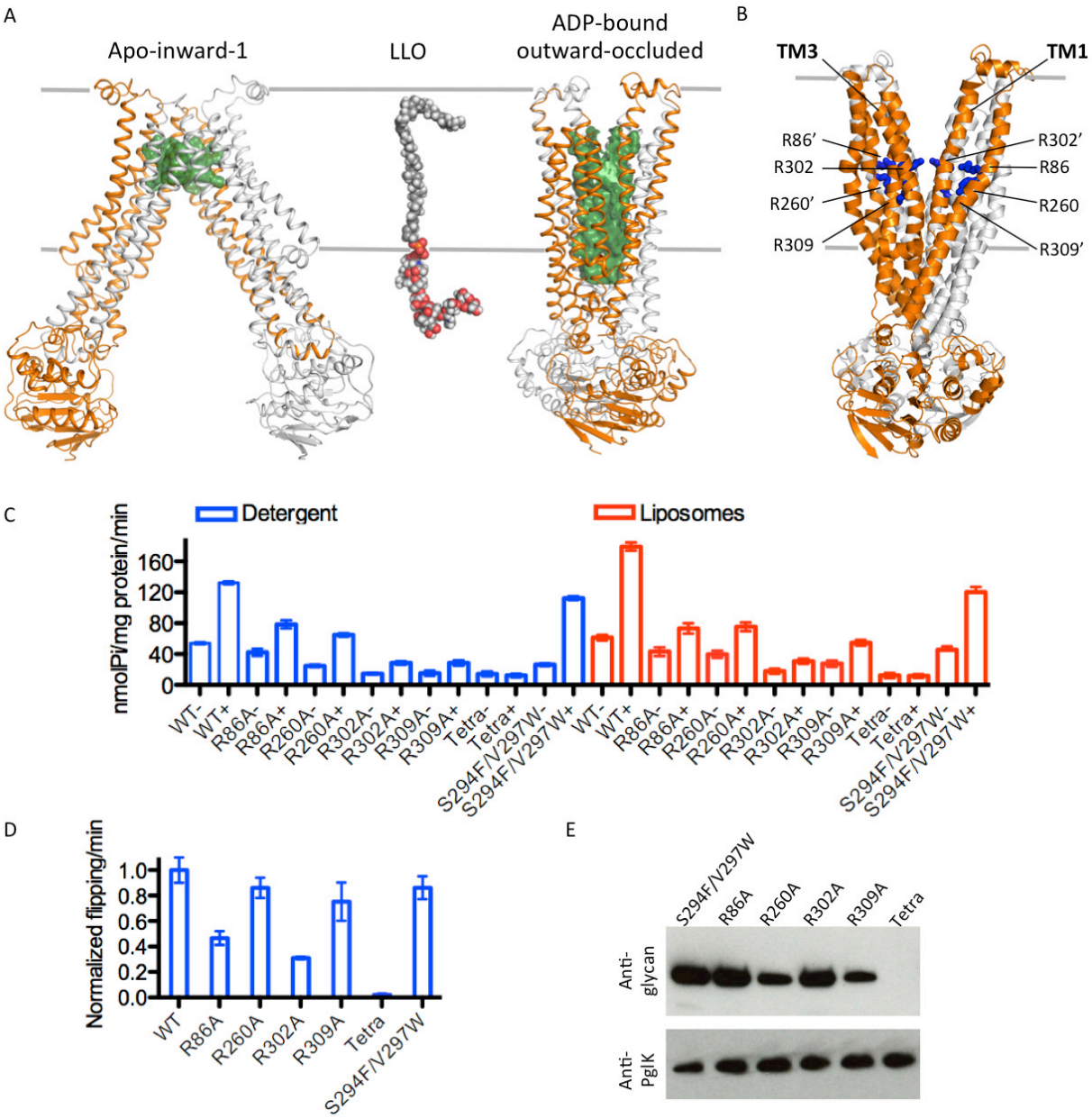
A
Apo-inward-1
LLO
ADP-bound
outward-occluded
B
TM3
TM1
R86'
R302
R260'
R309
R302'
R86
R260
R309'
C
Detergent
Liposomes
nmolPi/mg protein/min
160
120
80
40
0
WT-
WT+
R86A-
R86A+
R260A-
R260A+
R302A-
R302A+
R309A-
R309A+
Tetra-
Tetra+
S294F/V297W-
S294F/V297W+
D
Normalized flipping/min
1.0
0.8
0.6
0.4
0.2
0.0
WT
R86A
R260A
R302A
R309A
Tetra
S294F/V297W
E
S294F/V297W
R86A
R260A
R302A
R309A
Tetra
Anti-glycan
Anti-PglK

Fig. 5

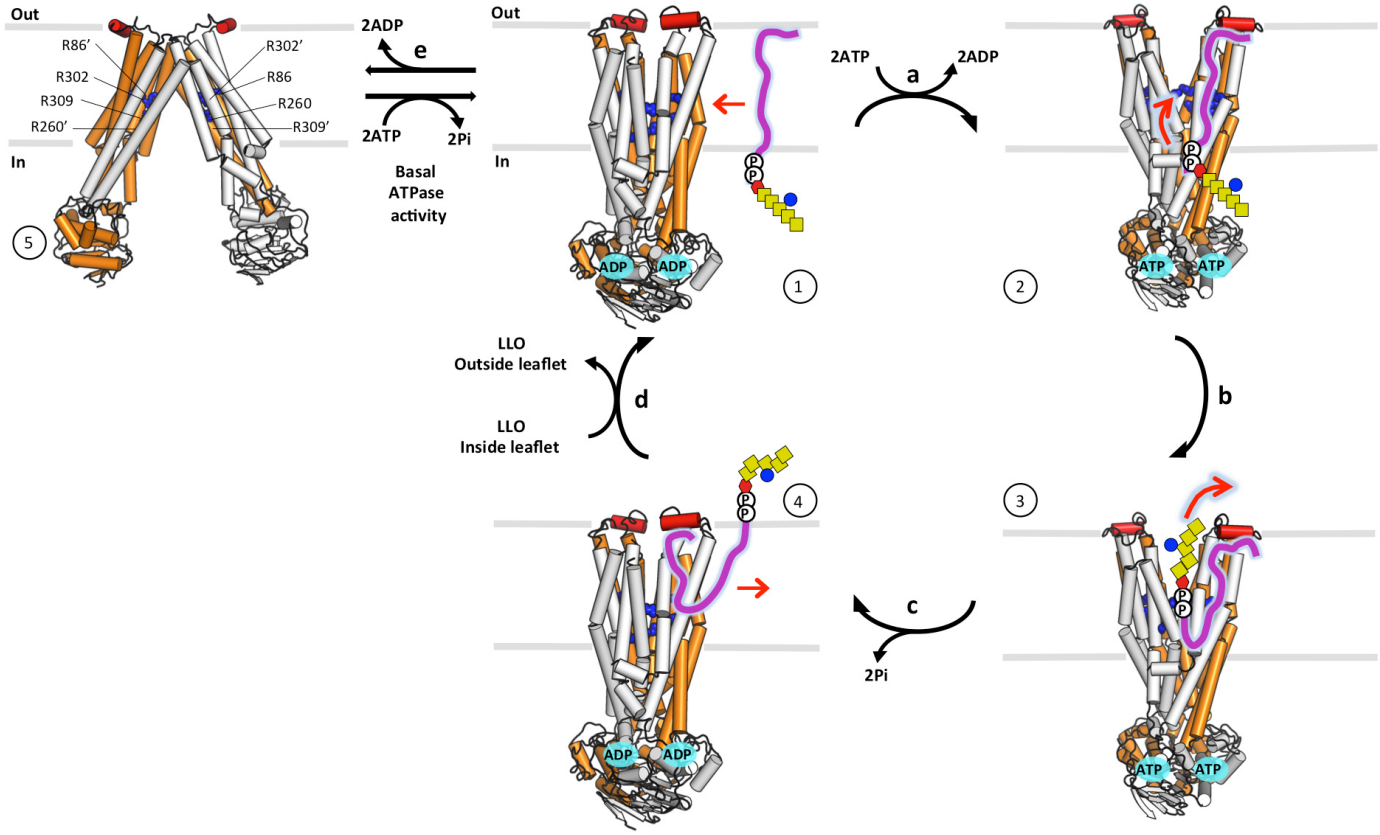
Out
R86'
R302'
R302
R86
R309
R260
R260'
R309'
In
5
2ADP
e
2ATP
2Pi
Basal
ATPase
activity
Out
In
ADP
ADP
1
2ATP
a
2ADP
2
ATP
ATP
b
LLO
Outside leaflet
d
LLO
Inside leaflet
4
ADP
ADP
c
2Pi
3
ATP
ATP

Extended Data Fig. 1

(LLO)
$GlcGalNAc_5Bac$-PP-Undecaprenyl

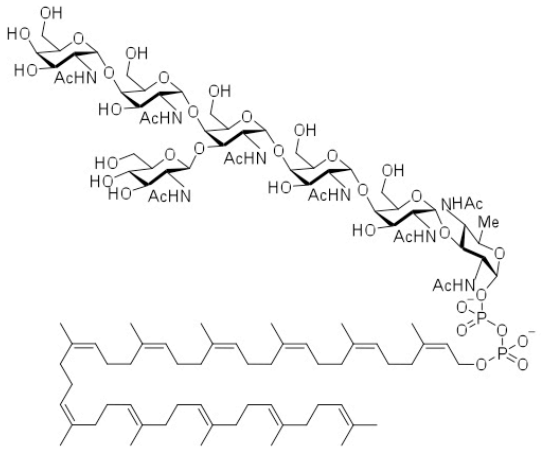

(tLLO)
$GalNAc_2Bac$-PP-Undecaprenyl

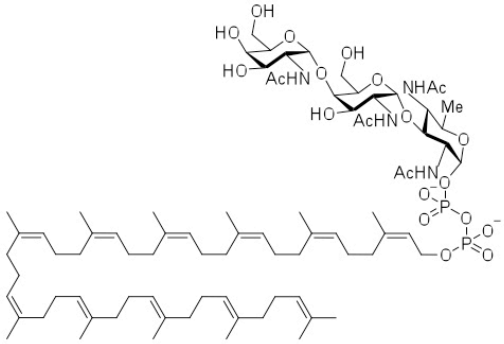

(GGPPGlcNAc)
GlcNAc-PP-Geranylgeranyl

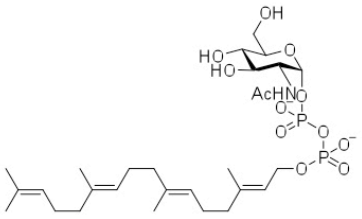

(FPPGlcNAc)
GlcNAc-PP-Farnesyl

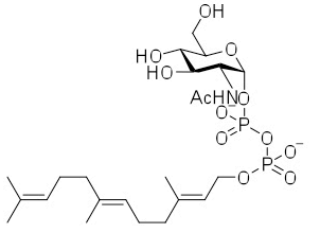

(FPP)
PP-Farnesyl

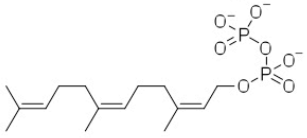

Ubiquinone

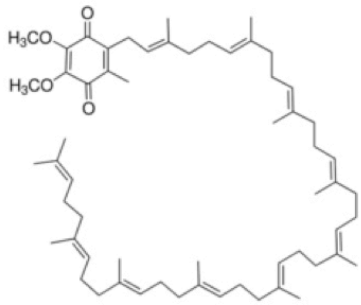

Extended Data Fig. 2

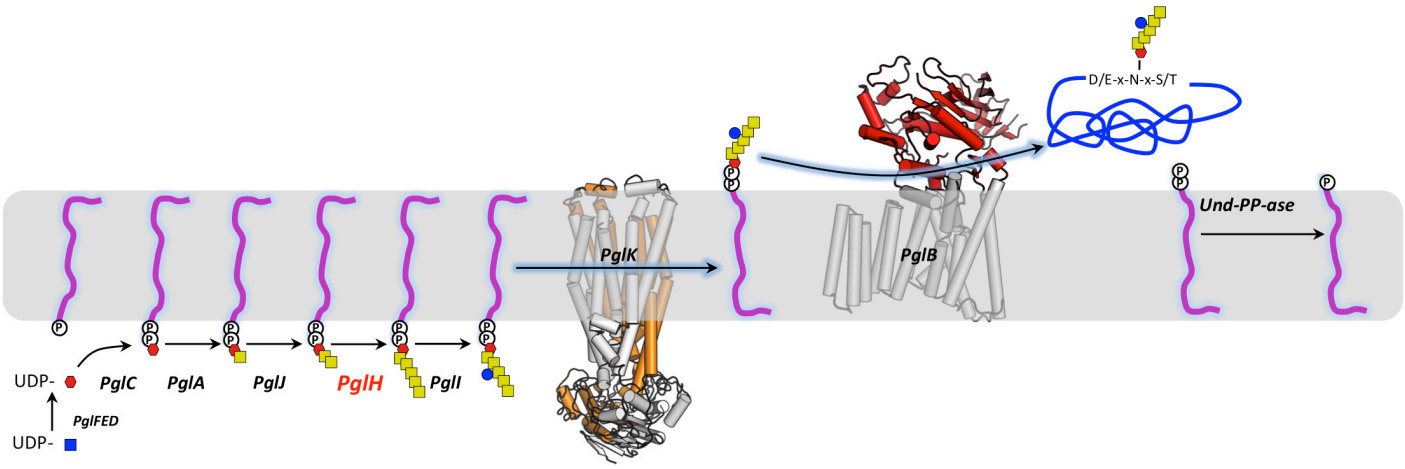

Extended Data Fig. 3

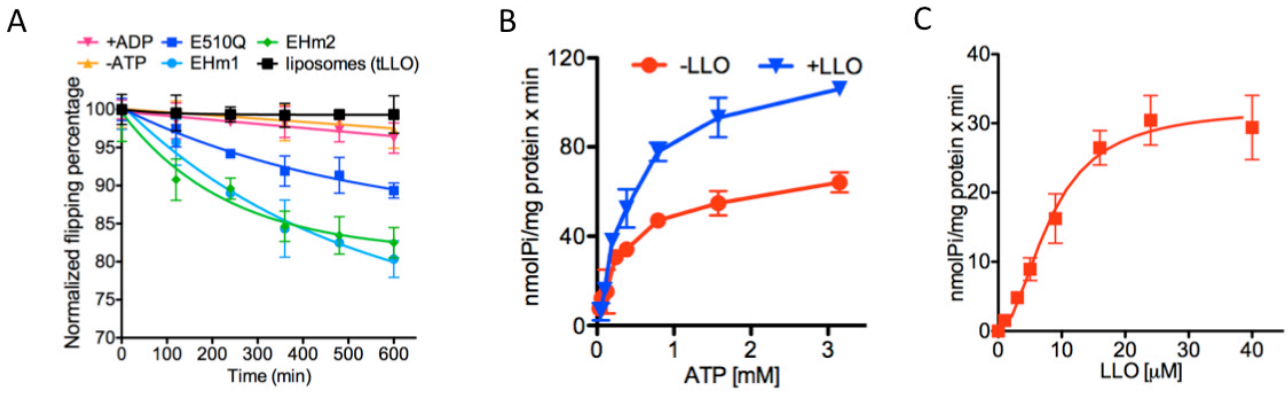

Extended Data Fig. 4

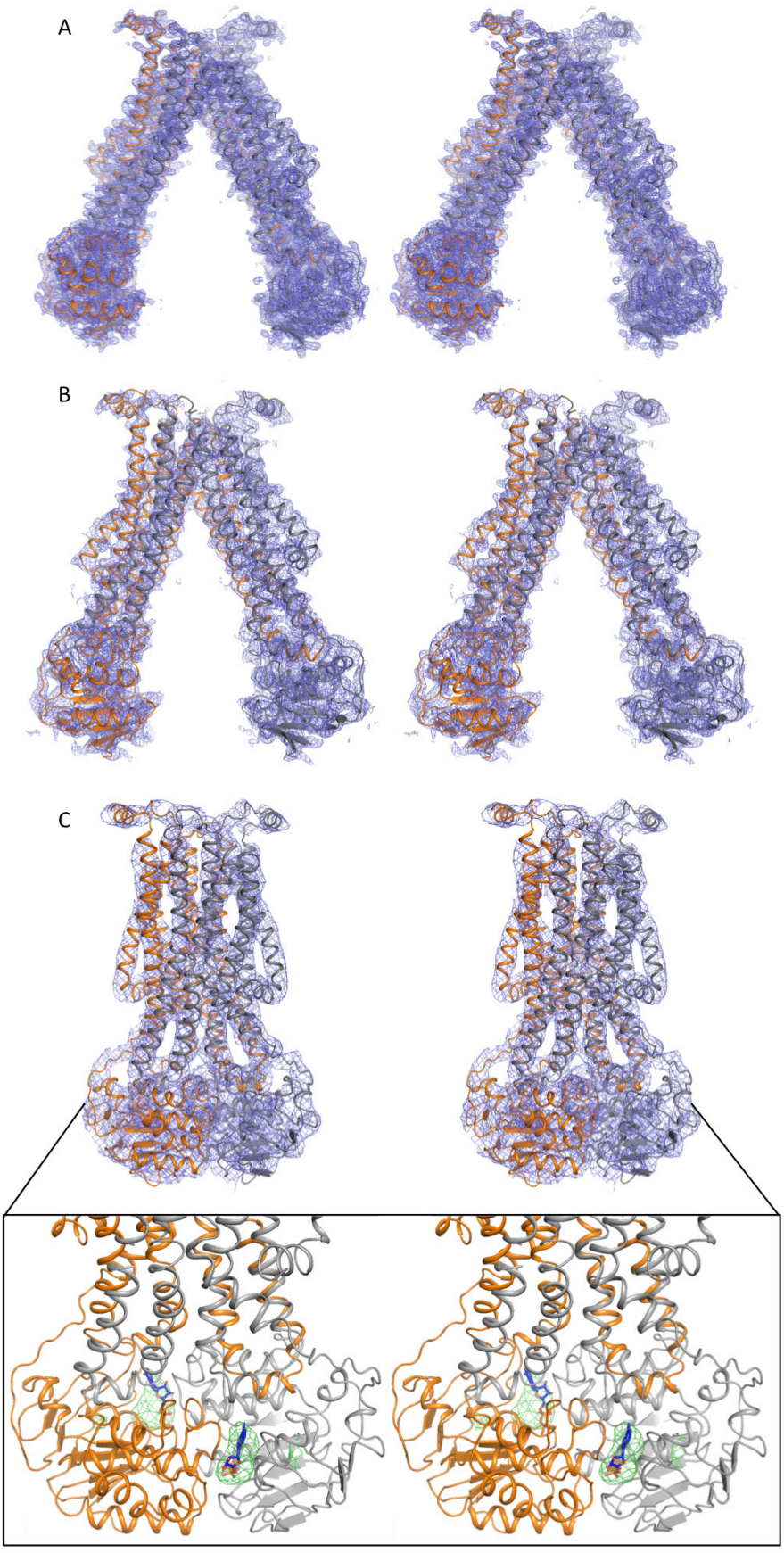

Extended Data Fig. 5

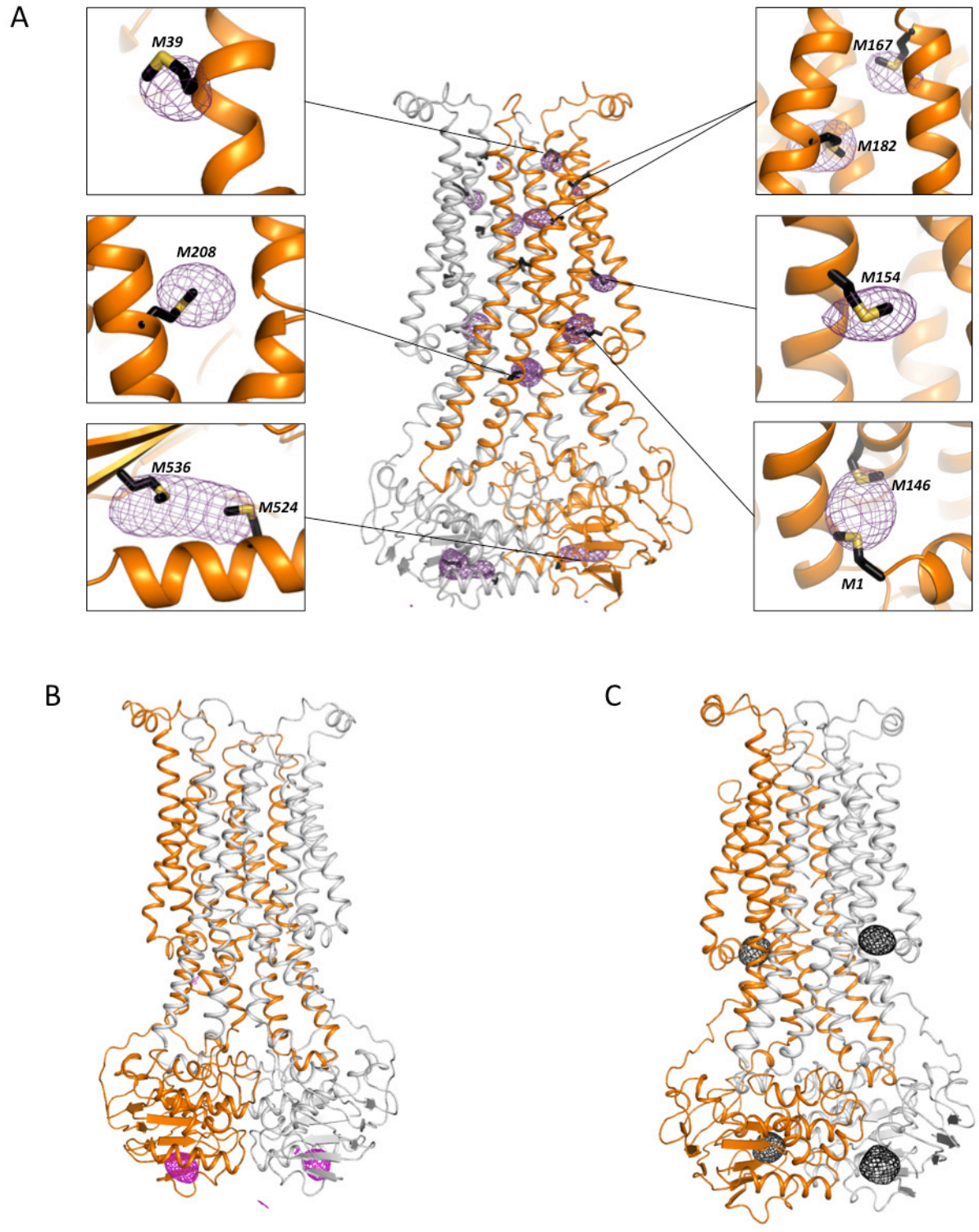

Extended Data Fig. 6

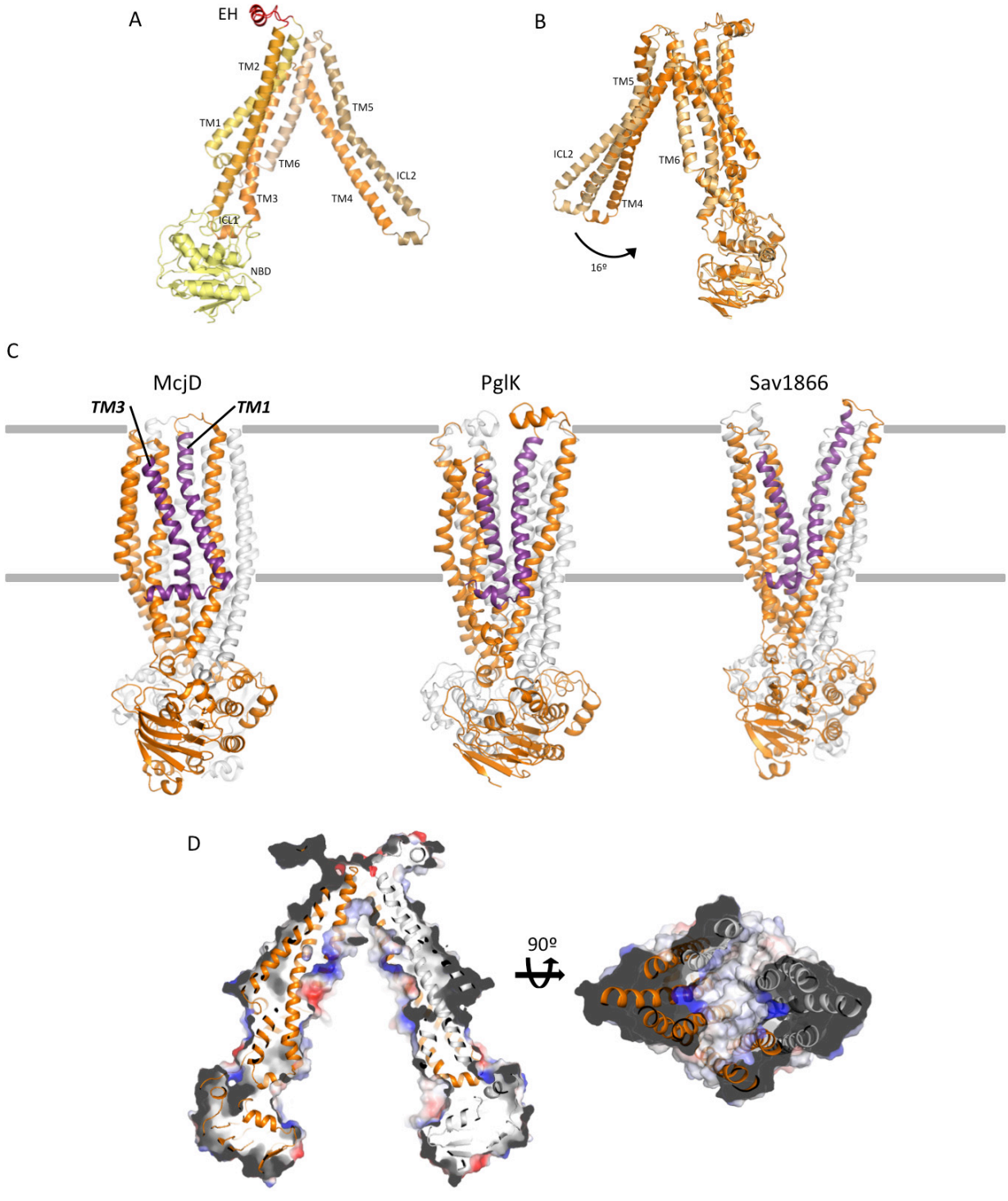

Extended Data Fig. 7

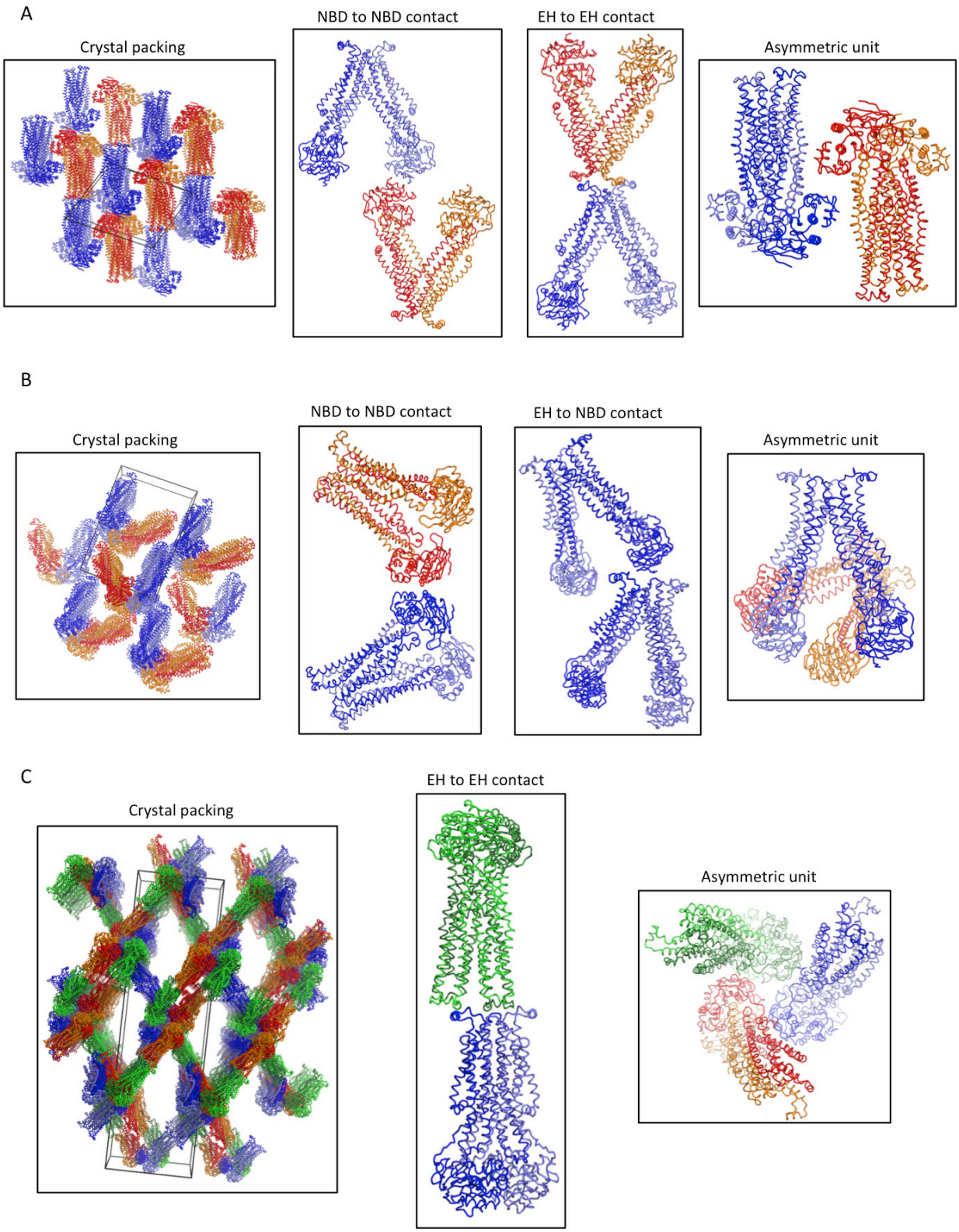

Extended Data Fig. 8

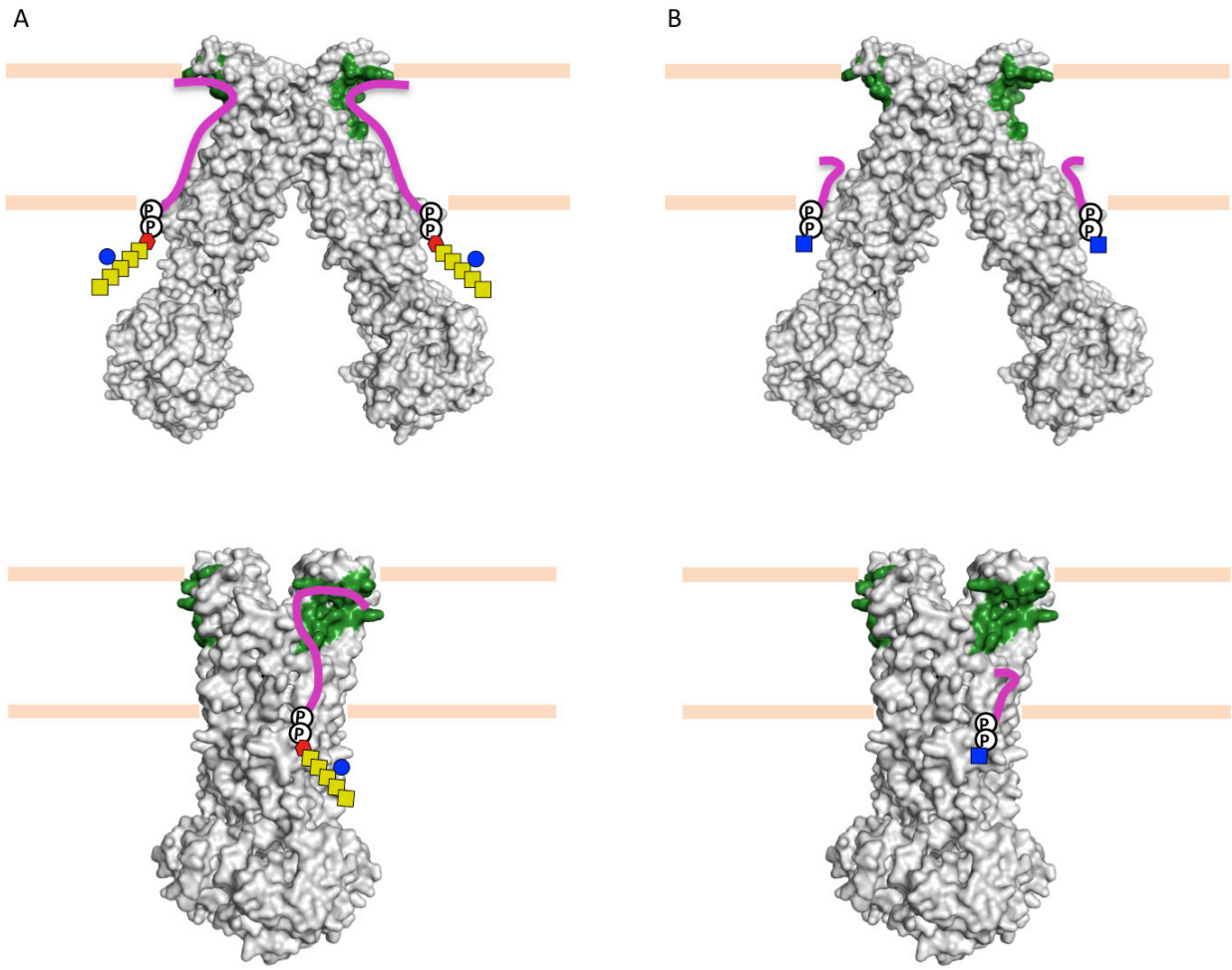

Extended Data Fig. 9

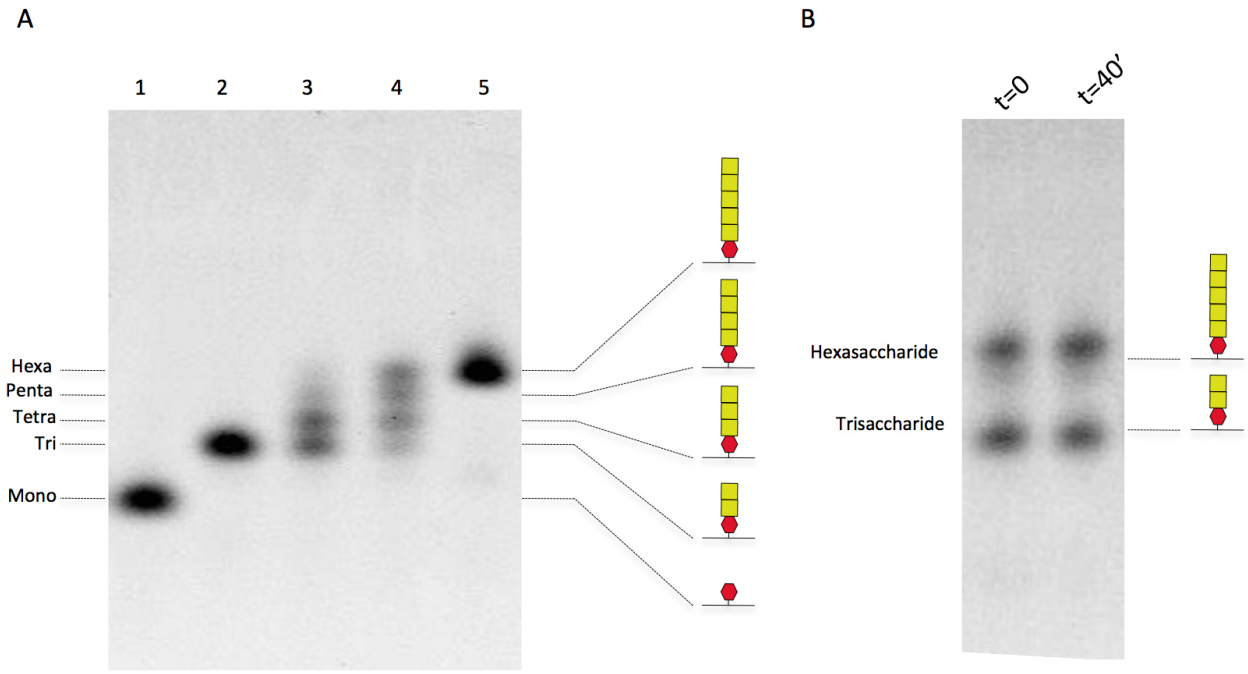

Extended Data Fig. 10

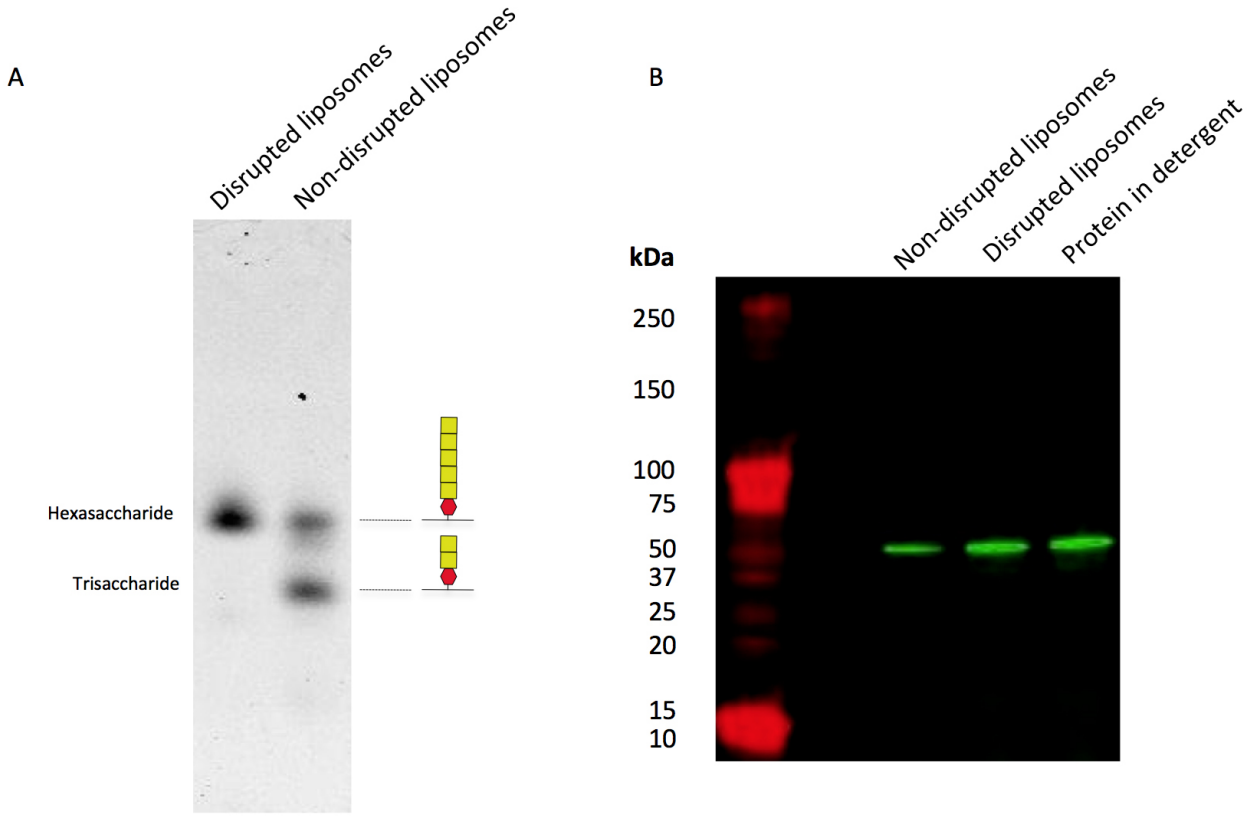

Extended Data Table 1 | X-ray data collection and refinement statistics

	Apo-inward-1 Native	Apo-inward-1 EMP	Apo-inward-2 Native	Out-occluded Native	Out-occluded SeMet	Out-occluded EMP	Out-occluded $PtCl_4^=$
Detergent	LMNG	LMNG	DDM	LMNG	LMNG	LMNG	LMNG
Data collection							
Wavelength (Å)	1.0000	1.0000	1.0000	1.0000	0.9779	1.0000	1.0722
Space group	P1	P1	$P12_11$	$P4_32_12$	$P4_32_12$	$P4_32_12$	$P4_32_12$
Unit cell:							
a/b/c (Å)	96.6/114.4/145.6	95.6/115.2/148.0	93.4/183.3/136.3	200.0/200.0/693.9	200.0/200.0/694.0	202.9/202.9/685.7	201.9/201.9/692.2
α/β/γ (°)	68.4/73.3/68.7	67.8/73.9/69.1	90/106.7/90	90/90/90	90/90/90	90/90/90	90/90/90
Resolution (Å)	30-2.9	30-3.3	30-3.9	30-5.9	30-6.7	30-6.4	30-6.9
Completeness (%)	87.20[99.3]	95.6	86.20[99.6]	84.56[98.3]	97.9	97.3	98.2
No. measured reflections	1176105[1457567]	421629	480068[804354]	1600808[2330114]	1527912	1591766	1540412
No. unique reflections	206754[258335]	206566	33489[60617]	60330[86104]	115835	118054	116442
I/σI	12.7(1.6)[10.4(0.6)]	6.55(1.55)	12.5(1.6)[11.1(0.3)]	18.1(2.0)[16(0.8)]	13.00(1.23)	8.45(1.13)	10.43(1.32)
R-merge (%)	11(140)[12(371)]		9.4(188)[11(158)]	20(257.4)[24(493)]			
$CC_{1/2}$ (%)	100(71)[100(51)]		100(70)[100(39)]	100(70)[100(42)]			
# of sites		12			54	6	12
Phasing power (iso./ano.)		0.557/0.788					
Figure of merit (FOM)		0.23/0.00*					
(acentric/centric)		0.86/0.00#					
Refinement							
R_{work}/R_{free} (%)	23.44/26.82		30.6/33.5	32.31/37.63			
CC* (%)	100(90)[100(80)]		100(82)[100(73.2)]	100(92.4)[100(78)]			
R.m.s.d. Bonds (Å)	0.011		0.006	0.012			
R.m.s.d. Angles (°)	1.558		1.005	1.635			
Ramachandran plot:							
Outliers (%)	5.69		5.69	7.48			
Allowed (%)	10.54		11.83	6.92			
Favored (%)	85.76		82.47	85.6			
Average *B*-factor ($Å^2$)	71.6		166.2	335.5			
Completeness (%)	87.4		86.4	84.6			

LMNG : lauryl maltose neopentyl glycol
DDM: dodecyl maltoside
Values in brackets are before anisotropic truncation (see below)
Values in parentheses are for the last resolution shell
$Rmerge = \Sigma_{hkl}\Sigma_i |I_i(hkl) - \langle I(hkl)\rangle| / \Sigma_{hkl}\Sigma_i I_i(hkl)$
*Before density modification
#After density modification

Extended Data Table 1, contd.

Anisotropic correction and ellipsoidal truncation of data sets

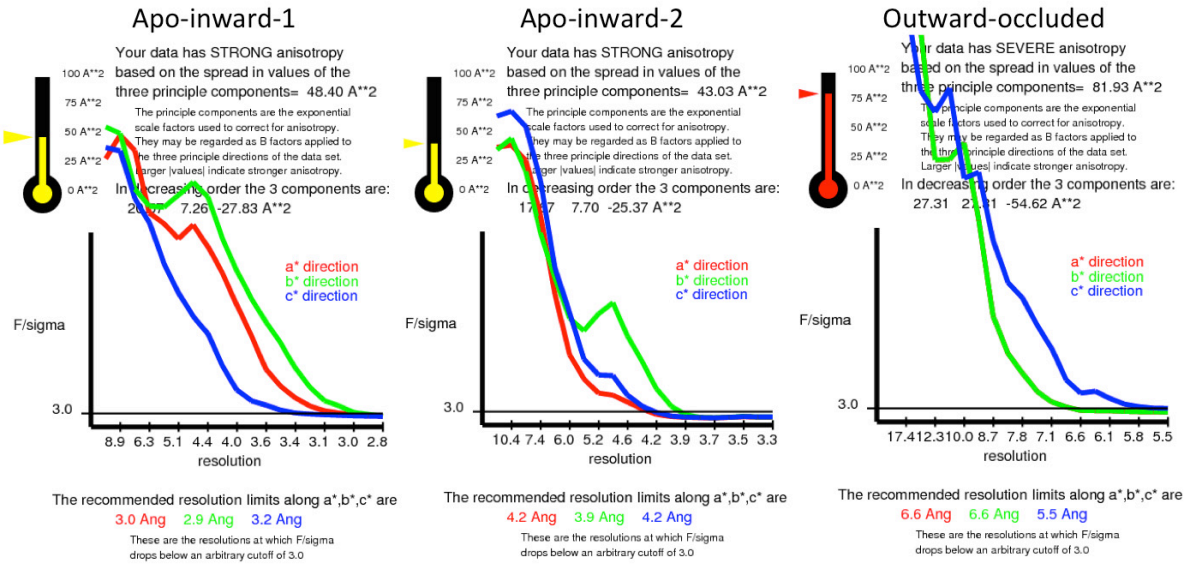

Methods

PglK expression and purification. The gene encoding PglK was cloned into a modified pET-19b vector (Novagen) with a N-terminal His_{10} affinity tag fused to PglK.

PglK from *C. jejuni* was overexpressed in *E. coli* BL21-Gold (DE3) (stratagene) cells in a 30 l fermentor (Infors). Cells were grown at 37ºC in modified Terrific Broth medium supplemented with 1% glucose (w/v) to A_{600} of 10.0 before the culture was induced by the addition of 0.2mM IPTG for 1h. All following steps were performed at 4ºC unless specified differently. Cells were harvested by centrifugation, re-suspended in 50mM Tris-HCl, pH 8.0; 500mM NaCl; 7mM β-mercaptoethanol; 0.5mM PMSF and disrupted in a M-110L microfluidizer (Microfluidics) at 15,000 p.s.i. chamber pressure. Membranes were pelleted by ultracentrifugation at 100,000g for 0.5h. PglK was solubilized in 50mM Tris-HCl, pH 8.0; 500mM NaCl; 20mM Imidazole; 15% glycerol (v/v); 7mM β-mercaptoethanol; 1% N-dodecyl-β-D-maltopyranoside (w/v) (DDM, Anatrace); 1% $C_{12}E_8$ anapoe (Anatrace) for 2h. The supernatant was loaded onto a NiNTA superflow affinity column (Qiagen), washed once with the same buffer but containing 10% glycerol (v/v); 50mM Imidazole; 0.016-0.03% DDM and then washed a second time with the same buffer containing 0.016-0.03% lauryl maltose neopentyl glycol (LMNG, affymetrix). Elution was performed in the same buffer containing 200mM NaCl; 200mM Imidazole. The protein was further purified by size exclusion chromatography (Superdex 200 10/300 GL, GE Healthcare) and fractions of peak were pulled together and concentrated to 8-10 mg/ml in an Amicon Ultra-15 concentrator (Millipore) with a molecular mass cutoff of 100kDa.

Seleno-methionine derivative production. PglK from *C. jejuni* was overexpressed in *E. coli* BL21 (DE3) RIPL (stratagene) cells. Briefly, cells in TB-glucose media were grown at 37 °C until OD 0.5-1.0. These were then used to inoculate a preculture of M9 media supplemented with vitamin B1 hydrochloride, cells were then grown until OD 0.5 and used

to inoculate 2 L M9 media supplemented with vitamin B1 hydrochloride. Cells were grown overnight at 37 ° until OD ~ 0.9. At that point an amino-acids SeMet cocktail was added to the cells and incubated during 30 minutes. Expression was then induced with 0.2 mM IPTG during 90 minutes. Cells were harvested immediately.

Native crystals. For crystallization of the outward-occluded state the protein was incubated for 0.5h with 5-10mM Adenosine 5′-diphosphate (ADP) and 5-10mM $MgCl_2$. The protein was crystallized by vapor diffusion in sitting drops or hanging drops at 20ºC against reservoirs containing 100mM Tris-HCl, pH 8.2; 150mM MgAcetate; 25% PEG400 for the apo-inward-1 state crystallization, 50mM Glycine-NaOH, pH 9.4; 300mM KCl; 50mM $MgCl_2$; 21% PEG600 for the apo-inward-2 state crystallization and 50mM Na/K phosphate, pH 7.5; 250mM NaCl; 3.5M Ammonium sulfate for the outward-occluded state crystallization. The protein to reservoir volume ratio was 2:1 – 1:1. Crystals typically appeared after 3–4 days and matured to full size within 2 weeks. Crystals were cryoprotected by gently increasing the cryoprotectant concentration in the drops (up to 30% PEG400 for apo-inward-1 and -2 and up to 3.0M ammonium sulfate for outward-occluded) and directly flash frozen by immersion in liquid nitrogen before data collection.

Heavy-metal derivatives. Native crystals were soaked for 1 day in 1mM ethyl mercury phosphate (EMP) or 1mM Potassium tetrachloroplatinate before back-soaking and flash-freezing by immersion in liquid nitrogen.

Data collection. Crystals belonged to the space groups, P1 (Apo-inward-1), $P2_1$ (Apo-inward-2) and $P4_32_12$ (outward-occluded). Native data were collected at the beamline X06SA at the Swiss Light Source (SLS, Villigen). EMP and $PtCl_4^=$ derivative data sets (**Extended Data Table 1**) were collected at the same station. Data were processed and merged with XDS[53] and anisotropic scaling/ellipsoid truncation was performed[54].

To improve the usable resolution and quality of the resulting electron density maps, we

used Karplus' CC* (Pearson's correlation coefficient) based data cutoff approach[55] (**Extended Data Table 1**). The resolution limit was set taking into account a $CC_{1/2}$>~40% based on data merging statistics and a CC* analysis against unmerged intensities in Phenix package[56] satisfying Karplus' CC* against CC-work and CC-free criteria, as well as, R-free of the highest resolution shell against the refined structure being less than or equal to ~50% (**Extended Data Table 1**).

Structures determination. Experimental phases of the apo-inward-1 structure were determined using multiple isomorphous replacement with anomalous scattering (MIRAS). Mercury positions were found using the SHELX computer program[57] and refined using the SHARP program[58]. Solvent flattening was performed using the program Solomon[59], and the phases were combined with a higher-resolution native data set using non-crystallographic symmetry averaging and solvent flatting. Electron density maps were calculated using CCP4 programs[60]. The protein model was built using Coot[61], and refined using Phenix[56]. X-ray data and refinement statistics are given in **Extended Data Table 1**.

The apo-inward-2 structure was solved by molecular replacement using a partial model from the apo-inward-1 structure as a search model using the program Phaser[62], refinement was performed using Phenix[56] combined with manual building in Coot[61]. The structure of the outward-occluded state was solved using a combination of molecular replacement using a partial model from the apo-inward-1 structure, and single wavelength anomalous dispersion (SAD) experiments on a selenomethionine derivative, and labeling of cysteine and histidine residues with EMP and $PtCl4^{=}$, respectively, in order to confirm the polypeptide chain register (**Extended Data Fig. 5A-C**). X-ray data and refinement statistics are given in **Extended Data Table 1**.

PglH expression and purification. The gene encoding PglH was cloned into a modified pET-19b vector (Novagen) with a N-terminal His_{10} affinity tag fused to PglH.

PglH from *C. jejuni* was overexpressed in *E. coli* BL21-Gold (DE3) (stratagene) cells in modified Terrific Broth medium supplemented with 1% glucose (w/v). Cells were grown at

37ºC to A_{600} of 3.0 before the culture was induced by the addition of 0.5mM IPTG and transfer to 18ºC for 16h. All following steps were performed at 4ºC unless specified differently. Cells were harvested by centrifugation, re-suspended in 50mM Tris-HCl, pH 8.0; 200mM NaCl; 20mM Imidazole; 0.5mM PMSF and disrupted in a M-110L microfluidizer (Microfluidics) at 15,000 p.s.i. chamber pressure followed by addition of 1% TritonX-100 (w/v)[32]. After centrifugation the supernatant was loaded onto a NiNTA superflow affinity column (Qiagen), washed once with the same buffer but containing 50mM Imidazole. Elution was performed in buffer containing 50mM Tris-HCl, pH 8.0; 500mM Imidazole. The protein was desalted into 50mM Tris-HCl, pH 8.0; 200mM NaCl.

LLO and tLLO extraction. Isolation of LLOs was performed as described by Gerber et al.[32]. Briefly, LLOs were extracted from *E. coli* SCM6 cells carrying a *Campylobacter jejuni* $pglB_{mut}$ cluster, containing an inactivated pglB gene (LLO extraction) or a $pglH_{mut}$:$pglB_{mut}$ cluster, containing an additionally inactivated pglH gene (tLLO extraction). Extraction was performed using a mixture of chloroform:MeOH:H2O, 10:10:3 (LLO) or MeOH:Chloroform 1:2 (tLLO). Extracts were dried in a rotavap and reconstituted in a buffer containing 10 mM Tris, pH 8.0, 150mM NaCl, and 1% Triton X-100 (w/v). The concentration of reconstituted LLOs was determined by titrating various amounts of LLOs against a constant amount of acceptor peptide in an *in vitro* glycosylation assay as described before[52].

Reconstitution of PglK and variants in preoteoliposomes. Liposomes (20 mg lipid ml^{-1}) from a mixture 3:1 (w:w) of *E. coli* polar lipids and L-α-phosphatidilcholine (Avanti polar lipids) were prepared by extrusion through polycarbonate filters (400 nm pore size) and diluted in 10mM Tris-HCl, pH8.0; 150mM NaCl; 2mM β-mercaptoethanol. After saturation with Triton X-100, the liposomes were mixed with purified protein at a lipid/protein ratio of 50-30:1 (w/w) and around tLLO. BioBeads were then added to remove detergent. Finally, proteoliposomes containing a final concentration of 20mg/ml lipids, 6.2-10.1µM

PglK and 20µM tLLO were centrifuged and washed before being frozen in liquid nitrogen and stored at -80°C.

Determination of PglK orientation in liposomes. The fully functional mutant of PglK (C269L/C352S/C386S/C549L/S544C), which contains one single cysteine residue at each NBD was reconstituted in proteoliposomes. After incubation with the thiol reacting Alexa Fluor® 488 C5 Maleimide fluorecent, samples were analyzed by SDS-PAGE. The ratio of PglK with NBDs facing outwards was calculated after comparison of the band intensities obtained from non-disrupted and disrupted proteoliposomes (0.3% Triton-X100). From this analysis we have concluded that 51.8 +/- 2.8 % of the PglK molecules are oriented with NBDs facing outwards.

***In vitro* tLLO flipping assay.** PglK proteoliposomes diluted in 10mM Tris-HCl, pH8.0; 150mM NaCl; 2mM β-mercaptoethanol were extruded through polycarbonate filters (400 nm pore size) and incubated with 5mM $MgCl_2$ and adenosine triphosphate (ATP) to initiate the tLLO flipping reaction. To stop the translocation reaction, samples were diluted into a buffer containing 4mM ADP. Labeling of non-flipped tLLO remnant in the external membrane leaflet of proteoliposomes was achieved after incubation with the glycosyltransferase PglH in the presence of 50µM [^{3}H]-UDP-GalNAc and 5mM $MnCl_2$. To stop the labeling reaction the samples were diluted into a cold stop buffer and filtered using Multiscreen vacuum manifold (MSFBN6B filter plate, Millipore). Radioactivity trapped on the filters was determined using a gamma counter (CobraII Auto-Gamma, Packard). Nonlinear fitting of data and initial velocities determination were performed using GraphPad Prism 5.

Product analysis and determination of tLLO orientation in liposomes. Glycosylation of tLLO was achieved after incubation of non-disrupted or disrupted proteoliposomes (0.3% Triton-X100), together with 3.5-50µM UDP-GalNAc, 2mM $MnCl_2$ and PglH 0.2 mg/ml. The polymerization reaction was stopped after heat shock (90°Cx10 minutes). The reaction

products of tLLO polymerization catalyzed by PglH were then analyzed by *in vitro* glycosylation of a fluorescently labelled substrate peptide (DQNAT sequon) catalyzed by PglB[32,33]. Briefly, the reaction products were incubated in a reaction mixture containing 10 mM MES, pH 6.5, 100 mM NaCl, 10 mM MnCl2, 3% glycerol (v/v), 1% Triton X-100 (w/v), 0.5 μM fluorescently labeled acceptor peptide and 1 μM PglB. The mixture was incubated at 30 °C. The reaction was stopped by the addition of 4xSDS sample buffer. Samples were analyzed by Tricine SDS-PAGE in minigels (8x8 cm) consisting of a 16% resolving gel with 6 M urea, a 10% spacer gel, and a 4% stacking gel[32,33]. Fluorescent bands for glycopeptide were visualized by using a Typhoon Trio Plus imager (GE Health-care) with excitation at 488 nm and a 526-nm SP emission filter. The amount of formed glycopeptide was determined from band intensities of fluorescence gel scans (ImageJ).

ATPase assays. ATP hydrolysis reactions were performed as described previously, using a modified molybdate-based colorimetric method[45]. Protein concentrations in the assays ranged from 0.1 mg/ml to 0.3 mg/ml. All reactions were performed in the presence of 2mM ATP (or a range of ATP concentrations for Km determination) and 5mM MgCl2. ATPase rates were determined using linear regression. Nonlinear regression and statistical analysis was performed using GraphPad Prism 5.

***In vivo* LLO flipping assay.** To analyze the flipping activity of PglK we have used a similar assay to that described before to measure PglB glycosylation activity *in vivo*[32]. PglK and variants were cloned into a pMLBAD plasmid[63] with a N-terminal His_{10} tag fused to it. This plasmid was transformed into *E. coli* cells defective for O-antigen biosynthesis (SCM6), carrying the plasmids pCL21[51] and pACYC-wlaB::kan[27]. pCL21 encodes for the expression of the single-chain Fv fragment of 3D5 carrying a DQNAT glycosylation site in the linker region and a C-terminal Myc tag fused to 3D5. pACYC-wlaB::kan codes for the biosynthesis of the *C. jejuni* lipid-linked-oligosaccharide (LLO) with a knockout of the *C. jejuni pglK* gene.

A 5 ml pre-culture was inoculated from a single clone and grown over night at 37°C in LB medium. The main culture was inoculated to an optical density A_{600} of 0.05 in 10 ml LB medium and grown at 37°C to A_{600} of 0.5. The culture was induced by addition of arabinose to 0.1% (w/v) and grown for 4h at 24°C. For extraction of periplasmic proteins, an equivalent of 1 ml culture volume with an A_{600} of 2 was harvested by centrifugation, re-suspended in 100 µl extraction buffer, consisting of 30 mM Tris-HCl, pH 8.5; 20% (w/v) sucrose; 1 mM EDTA and 1 mg/ml lysozyme (Sigma) and incubated for 1 h at 4°C. A final centrifugation step yielded periplasmic proteins in the supernatant. Glycosylation of 3D5 and expression of PglK were analyzed by immunoblot following SDS–PAGE. Immunodetection was performed with anti-glycan serum hR6[19] to observe glycosylated 3D5. Immunodetection of *C. jejuni* PglB was performed with anti-His-HRP serum (Sigma).

Mutagenesis. PglK mutants were generated by either the QuickChange method or using gBlocks® gene fragments (Integrated DNA technologies). The resulting plasmids of all constructs were validated by DNA sequencing (Microsynth). PglK variants were cloned into pMLBAD as above and used in flipping *in vivo* assays.

Truncated LLOs synthesis. Farnesyl- and geranylgeranyl-PP-GlcNAc were synthesized in seven steps from commercially available lipids and sugar according to the strategy of Davis et al. with slight modifications[52]. As the procedure involves the formation of highly acid sensitive phosphorylated intermediates, flash column chromatography were performed on silica gel basified with an ammonium hydroxide solution to avoid product degradation during purification. The final LLOs were obtained from the protected precursor by deacetylation using an ammonium hydroxide solution in methanol for 6h. After freeze-drying, 16 mg of farnesyl-PP-GlcNAc and 42 mg of geranylgeranyl-PP-GlcNAc (5% overall yield from the lipid) were respectively isolated as final compounds and were shown to be pure by ^{1}H, ^{13}C, ^{31}P NMR as well as negative mode ESI-HRMS.

53. Kabsch, W. Xds. *Acta Crystallogr D Biol Crystallogr* **66**, 125-32 (2010).
54. Strong, M. et al. Toward the structural genomics of complexes: crystal structure of a PE/PPE protein complex from Mycobacterium tuberculosis. *Proc Natl Acad Sci U S A* **103**, 8060-5 (2006).
55. Karplus, P.A. & Diederichs, K. Linking crystallographic model and data quality. *Science* **336**, 1030-3 (2012).
56. Adams, P.D. et al. PHENIX: a comprehensive Python-based system for macromolecular structure solution. *Acta Crystallogr D Biol Crystallogr* **66**, 213-21 (2010).
57. Sheldrick, G.M. A short history of SHELX. *Acta Crystallogr A* **64**, 112-22 (2008).
58. Bricogne, G., Vonrhein, C., Flensburg, C., Schiltz, M. & Paciorek, W. Generation, representation and flow of phase information in structure determination: recent developments in and around SHARP 2.0. *Acta Crystallogr D Biol Crystallogr* **59**, 2023-30 (2003).
59. Abrahams, J.P. & Leslie, A.G. Methods used in the structure determination of bovine mitochondrial F1 ATPase. *Acta Crystallogr D Biol Crystallogr* **52**, 30-42 (1996).
60. Collaborative Computational Project, N. The CCP4 suite: programs for protein crystallography. *Acta Crystallogr D Biol Crystallogr* **50**, 760-3 (1994).
61. Emsley, P., Lohkamp, B., Scott, W.G. & Cowtan, K. Features and development of Coot. *Acta Crystallogr D Biol Crystallogr* **66**, 486-501 (2010).
62. McCoy, A.J. et al. Phaser crystallographic software. *J Appl Crystallogr* **40**, 658-674 (2007).
63. Lefebre, M.D. & Valvano, M.A. Construction and evaluation of plasmid vectors optimized for constitutive and regulated gene expression in Burkholderia cepacia complex isolates. *Appl Environ Microbiol* **68**, 5956-64 (2002).